JCI The Journal of Clinical Investigation

Mef2d sustains activation of effector Foxp3+ Tregs during transplant survival and anticancer immunity

Eros Di Giorgio, … , Ulf H. Beier, Wayne W. Hancock

J Clin Invest. 2020. https://doi.org/10.1172/JCI135486.

Research In-Press Preview Immunology Oncology

Graphical abstract

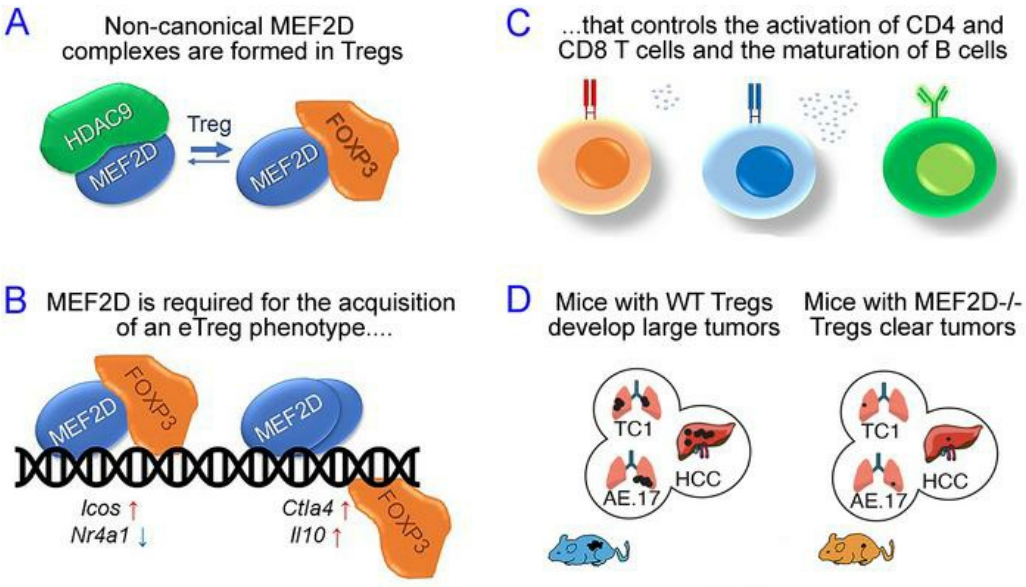

Mef2d sustains activation of effector Foxp3+ Tregs during transplant survival and anticancer immunity

Eros Di Giorgio,[1a] Liqing Wang,[1a] Yan Xiong,[1,2] Tatiana Akimova,[1] Lanette M. Christensen,[1] Rongxiang Han,[1] Arabinda Samanta,[1] Matteo Trevisanut,[1] Tricia R. Bhatti,[3] Ulf H. Beier,[4] and Wayne W. Hancock[1*]

[1]Division of Transplant Immunology, Department of Pathology and Laboratory Medicine, Children's Hospital of Philadelphia and Perelman School of Medicine, University of Pennsylvania, Philadelphia, Pennsylvania, USA.

[2]Institute of Hepatobiliary Diseases of Wuhan University, Transplant Centre of Wuhan University, Zhongnan Hospital of Wuhan University, Wuhan University, Wuhan, China.

[3]Division of Anatomical Pathology, Department of Pathology and Laboratory Medicine, Children's Hospital of Philadelphia and Perelman School of Medicine, University of Pennsylvania, Philadelphia, Pennsylvania, USA.

[4]Division of Nephrology, Department of Pediatrics, Children's Hospital of Philadelphia and Perelman School of Medicine, University of Pennsylvania, Philadelphia, Pennsylvania, USA.

Conflict of interest: The authors have declared that no conflict of interest exists.

[a]These authors contributed equally.

***Correspondence:** Wayne W. Hancock, Children's Hospital of Philadelphia, 916B Abramson Research Center, 3615 Civic Ctr Blvd, Philadelphia, Pennsylvania 19104. Phone: 215-590-8709; Email: whancock@pennmedicine.upenn.edu

Abstract

The transcription factor, Mef2d, is important in the regulation of differentiation and adaptive responses in many cell types. We found that among T cells, Mef2d gained new functions in Foxp3+ T-regulatory (Treg) cells due to its interactions with the transcription factor, Foxp3, and its release from canonical partners, like histone/protein deacetylases. Though not necessary for the generation and maintenance of Tregs, Mef2d was required for the expression of IL-10, Ctla-4 and Icos, and for the acquisition of an effector Treg phenotype. At these loci, Mef2d acted both synergistically and additively to Foxp3, and down-stream of Blimp1. Mice with the conditional deletion in Tregs of the gene encoding Mef2d were unable to maintain long-term allograft survival despite costimulation blockade, had enhanced antitumor immunity in syngeneic models but displayed only minor evidence of autoimmunity when maintained under normal conditions. The role played by Mef2d in sustaining effector Foxp3+ Treg functions without abrogating their basal actions suggests its suitability for drug discovery efforts in cancer therapy.

Introduction

The roles played by T-regulatory (Treg) cells in the maintenance of immune homeostasis are well established (1). By restricting T cell functions, Tregs restrain the onset of autoimmunity but also dampen anti-cancer immunity (2). The transcription factor Foxp3 is required but not sufficient to sustain the immunosuppressive properties of Tregs (3). Pioneering factors (4-6) pave the way for Foxp3 expression in concert with a large number of epigenetic regulators that modulate its activities (7-13).

Beside the assembly and regulation of large multiprotein complexes containing Foxp3, the execution and the sustainment of the Treg program requires the activation of other transcription factors that act as genetic modulators (14). The action of these transcription factors may be supportive to Foxp3, like Thpok (15), or may be independent and additive or subtractive to Foxp3 (14). In particular, the co-expression of master transcription factors along with Foxp3 marks some Treg subsets, e.g. colonic Tregs co-expressing RORγt and Foxp3 (16, 17), or follicular Tregs (Tfr) co-expressing Bcl6 and Foxp3 (18, 19). In these various Treg subsets, the sum of the genetic responses triggered by the simultaneous activation of multiple master factors lets them acquire functional nuances more suited to their location (20). In other cases, in response to certain stimuli the activation of transcription factors such as Blimp1 and Irf4 can synergize with Foxp3 and trigger a reinforced Treg program that characterizes so-called effector Tregs (eTregs) (21).

Mef2d belongs to the MEF2 (Myocyte Enhancer Factor-2) family of transcription factors (22). The weak intrinsic transcriptional activity of Mef2d can be potentiated by the binding of co-activators, like p300 (23), or completely blocked or even converted into transcriptional repression by the actions of co-repressors, like class IIa histone/protein deacetylases (HDACs) (24). The great plasticity of MEF2 transcription factors allows the precise modulation of differentiative and adaptive responses (22). Moreover, their binding to tissue-specific co-factors allow MEF2 transcription factors to play key roles in supervising the transcriptional program that underlies heterogeneous processes such as muscle differentiation, ossification, cardiac hypertrophy, synaptogenesis and lymphoid commitment (22).

Mef2d is known to be highly expressed in T cells (25). In activated T cells, Mef2d sustains the production of IL-2 (26, 27), IL-4 and IFN-γ (28), as a consequence of its release from class IIa HDACs and Cabin1 inhibition (26-28). In the thymus, Mef2d regulates the negative selection of double-positive T cells by promoting the transcription of Nurr77 in an HDAC7-dependent manner (29). Moreover, the inhibition or the knock-out of the MEF2 repressor Hdac9 increases the suppressive properties of Treg cells (30), at least in part by sustaining the metabolic switch to OXPHOS that is characteristic of these CD4+Foxp3+ cells (31). Conversely, the expression of a gain of function mutant of Hdac7 decreases the proportion of Tregs (32).

In this study, we analyzed the still unexplored roles of Mef2d in CD4+ Foxp3+ Treg cells. We focused on Mef2d since it was by far the most expressed member of the Mef2 family of paralogs in both human and murine Tregs. We found that Mef2d interacts with Foxp3 and modulates its activities, but also exerts Foxp3-independent functions required for Treg fitness. In addition, depletion of Mef2d in Treg cells dampens the Foxp3 program, especially in supraphysiological conditions that stimulate inflammation, such as transplantation and cancer.

Results

Foxp3 controls the expression and alternative splicing of Mef2d. Human and murine CD4+ Foxp3+ Tregs express high levels of Mef2d (Supplemental Fig. 1A & B, respectively), and Foxp3 binds to the promoter of Mef2d in both human and murine Tregs (Supplemental Fig. 1C & D). Comparison of Mef2d mRNA and protein levels in T-effector (Teff) and Treg cells from C57BL/6 mice shows ~2-fold more Mef2d in Treg cells (Fig. 1A & B). We noticed that the genomic region of MEF2D encoding the two alternative third exons (3α1 and 3α2, Fig. 1C) has chromatin features (H3K27ac and H3K36me3) typical of their active splicing in human Tregs but not in Teff cells (Supplemental Fig. 1E). Moreover, the α2 isoform of Mef2d is reported to be expressed not only in muscle cells and neurons, but also in the spleen (33). We confirmed that the slight increase in Mef2d levels observed in freshly isolated Tregs in respect to Teffs is at least in part due to the expression of the α2 isoform (Fig. 1D & E). This increase is stronger after 24 h of stimulation with CD3/CD28 and IL-2 (Fig. 1D & E). In these conditions, a slight increase in the α1 transcript can also be observed (Fig. 1D), probably as a consequence of higher transcriptional activity on the Mef2d promoter. However, differently from the α2 isoform, the protein levels of the α1 isoform are not increased after stimulation, likely as a consequence of the increased instability of this isoform that selectively undergoes proteasomal degradation (34). Foxp3 is necessary to trigger the expression of the α2 isoform since suppression of Foxp3 leads to significant decreases in the mRNA and protein levels of the α2 isoform, while the α1 isoform is minimally affected (Fig. 1G, H & I). Moreover, prolonged stimulation for 60 h with CD3/CD28 mAbs and IL-2 stimulates the transcription of both the α1 and α2 isoforms of Mef2d, though with different magnitudes (2 and 10 times, respectively) (Fig. 1F). While the α1 isoform is reported to be widespread though all the tissues of the body, the α2 isoform has a restricted pattern of expression and influences differentiative (35, 36) and adaptative (37, 38) responses. Moreover, compared to the α1 isoform, the α2 isoform encodes for a stronger transcription factor since it lacks the phosphorylation sites of PKA (36) and CDK4/6 (34) that mediate the inhibition or proteasomal degradation of Mef2d. We conclude that, in contrast to Teffs, Tregs are characterized by an increase in Mef2d levels and by the Foxp3-dependent expression of the α2 isoform of Mef2d.

Foxp3 influences the assembly of Mef2d complexes. Foxp3 forms multiprotein complexes containing different

transcription factors (7, 39). To test whether Mef2d can be part of such complexes, we transfected 293 cells with the α1 isoform of Mef2d, p300 and Foxp3. As shown in Fig. 1J, Mef2d is stabilized by the co-expression of p300, and it interacts with both p300 and Foxp3, while the co-expression of Foxp3 and p300 does not perturb their binding to Mef2d (Fig. 1J). Foxp3 does not bind to the DNA binding domain of Mef2d, as the deletion of this region does not abolish their interaction (Fig. 1K). Moreover, the immunoprecipitation (IP) of Mef2d leads to co-IP of Foxp3 in both freshly isolated and stimulated Tregs (Fig. 1L). Mef2d binds strongly to p300 both in Teffs and in Tregs (resting or activated), while its binding to Hdac3 and Hdac9 is decreased in Tregs compared to Teffs, and respectively severely impaired or abolished after stimulation (Fig. 1L). This could be also due to the decreased protein levels of Hdac3 and Hdac9 observed after stimulation (Fig. 1L). We hypothesized that the different stoichiometry of Mef2d complexes between Tregs and Teffs could be due to the increased α2 isoform observed in Foxp3+ cells. This was the case, since in freshly purified Tregs only the α1 isoform of Mef2d interacted strongly with Hdac9, whereas Foxp3 preferentially interacted with the α2 isoform (Fig. 1M). To further assess these interactions, we transfected 293 cells with the two isoforms of Mef2d plus Foxp3 or Hdac9, and we pulled-down Mef2d with isoform-specific antibodies (Fig. 1N). We found that the α2 isoform of Mef2d interacts strongly with Foxp3 and weakly with Hdac9 compared to the α1 isoform (Fig. 1N). In reciprocal studies, IP of Foxp3 led to co-IP of Mef2d (Fig. 1O). We conclude that in Tregs, different complexes assemble on Mef2d isoforms in response to Foxp3 expression and exogenous stimulation.

Characterization of Tregs deficient for Mef2d. Two different complexes assemble on Mef2d in Tregs. Only one, mainly associated with the α1 isoform, contains strong repressors like Hdac9. We hypothesized that both of these complexes are required to maintain Treg immune suppressive properties; the first, “the repressive one” might be required to switch off some Mef2d genetic programs, while the second one might sustain and promote the expression of Treg-specific genes. To prove this concept, we conditionally deleted Mef2d in Foxp3+ Treg cells by crossing $Mef2d^{fl/fl}$ mice (40) and $Foxp3^{YFP/Cre}$ mice. The KO allele encodes for a protein with an in-frame deletion of the second exon that is involved in DNA binding and dimerization leading to the complete loss of function of the protein (40, 41). $Mef2d^{fl/fl}Foxp3^{YFP/Cre}$ (hereafter Mef2d-/-) mice were born at expected Mendelian ratios and appeared to develop normally over 1 year of monitoring. However, histologic examination of tissues

from Mef2d-/- mice were characterized by the presence of mild mononuclear cell infiltrates in the lung and liver, while they did not show any defects in colon, skin, pancreas, thymus or other tissues (Supplemental Fig. 2). Gene deletion was assessed by purifying Treg cells from WT and Mef2d-/- mice and confirming Mef2d deletion by immunoblot (Fig. 2A). Moreover, as expected, the depletion of a functional Mef2d protein impaired the expression of the Mef2d target gene, Hdac9 (Fig. 2A). We further characterized the Mef2d-/- mice by harvesting secondary lymphoid tissues and assessing their cell populations by flow cytometry. Mef2d-/- mice were characterized by increased proportions of CD4+Foxp3+ Tregs within lymph nodes, spleen and thymus (Fig. 2B & C), and by increased proportions of splenic CD4+CD69+ cells (Fig. 2D & E). While no significant alterations were observed in CD8 subpopulations (data not shown), increased proportions of CD4+Foxp3- effector memory cells ($CD44_{hi}CD62L_{lo}$) were observed within lymph nodes, spleen and thymus (Fig. 2F & G). Nevertheless, the *in vitro* suppressive functions of Tregs from Mef2d-/- mice were not significantly impaired compared to WT Tregs in standard Treg assays (Fig. 2H & I), though they did display modestly impaired suppression of CD4+ and CD8+ when using bulk WT splenocytes as responder cells (Fig. 2J). Altogether, these features are indicative of a modest inflammatory state in Mef2d-/- mice but one that is insufficient to provoke significant autoimmunity under basal conditions.

Mef2d-specific and Foxp3-specific signatures are altered in Mef2d-/- Tregs. The transcriptomes of WT and Mef2d-/- Tregs were analyzed by RNA-seq. Mef2d deletion caused the up-regulation of 795 transcripts and the repression of 700 genes (>1.3-fold, $p<0.05$) (Fig. 3A). Gene set enrichment analysis (GSEA) showed that four main signaling pathways were altered in Mef2d-/- Tregs: i) DNA repair (Fig. 3B and Supplemental Fig. 3A); ii) E2F targets/proliferation (Fig. 3C and Supplemental Fig. 3B); iii) PPAR/RA signaling (Fig. 3D and Supplemental Fig. 3C); and iv) TREG signature (Fig. 3E & F and Supplemental Fig. 3D & E). The first three were severely impaired in Mef2d-/- Tregs and belong to the general core responses regulated by MEF2 transcription factors (22). Analysis of the Treg signature (42) showed that key genes induced in Treg versus Teff cells were indeed repressed in Mef2d-/- Tregs (Fig. 3E), and conversely, transcripts normally repressed in Tregs were up-regulated in Mef2d-/- Tregs (Fig. 3F). We validated by qPCR (Fig. 3H) and immunoblot (Fig. 4A) changes in expression the main hubs involved in the identified altered pathways. We confirmed by different methods an impairment in

the proliferation of Mef2d -/- Tregs (Fig. 4B-D and Supplemental Fig. 4A-C), that appears at least partially due to a prolonged quiescence rather than senescence (Fig. 4C), even if a moderate impairment in cellular fitness cannot be excluded.

Mef2d-/- Tregs lose the hallmarks of eTregs. Foxp3 is expressed in Mef2d-/- Tregs at levels comparable to control mice (Fig. 4A). However, Mef2d-/- Tregs show reduced levels of three genes (*Ctla4, Icos* and *Il10)* that encode proteins centrally involved in the immunosuppressive functions of Tregs (Fig. 3G & 4A). High levels of these proteins are a feature of so-called highly suppressive effector Tregs (eTregs) (43) that are dependent on Blimp1 (21) and Irf4 (44). GSEA performed on the transcriptome of Mef2d-/- Tregs confirmed their inverse correlation with Blimp1+ Tregs (Fig. 5A & B); in particular, key genes induced in Blimp1+ cells were significantly repressed in Mef2d-/- Tregs (Fig. 5C). We validated by qPCR (Fig. 3G) and flow cytometry (Fig. 5D-F and Supplemental Fig. 4F) the downregulation in Mef2d-/- Tregs of Ctla4, Icos and IL-10; the latter is especially impressive in stimulated cells (Fig. 5G). As a consequence, Teff cells were more active in Mef2d-/- mice (Fig. 2F & G).

Blimp1 expression is not altered in Mef2d-/- cells (Fig. 5H), and Mef2d expression is not altered in Blimp1-/- Tregs (GSE84827, Supplemental Fig. 5A) (45). Moreover, Blimp1 does not interact with Mef2d, but does pull-down its well-known interactor, Hdac2 (46) (Supplemental Fig. 5B). However, Hdac9 is repressed in Blimp1+ Tregs (GSE103456, Supplemental Fig. 5C) (47) and is induced in Blimp1-/- Tregs (GSE84827, Supplemental Fig. 5A) (45). This suggests that in Blimp1+ Tregs, Mef2d is released from its inhibitors. Indeed, many Blimp1 target genes are bound by MEF2 at their proximal promoters (Table 1). We hypothesized that Mef2d acts downstream to Blimp1 and is required to sustain the high repressive properties of eTregs. As expected, the suppressive properties of Foxp3+ Mef2d-/- Tregs were only partially enhanced after their pre-activation with CD3/CD28, differently from WT (Fig. 5I-J). This defect may be partially due to a moderately increased susceptibility of Mef2d-/- Tregs to apoptosis as seen *in vitro* (Supplemental Fig. 5D & E). These features, collectively, are typically associated with an impairment of eTreg functions (48). A similar trend was also seen by Tregs, expanded *in vivo* by IL-2, in Treg assays (Supplemental Fig. 5F-I).

Conditional Treg deletion of Mef2d affects Tfr and Tfh cells and B-cell maturation in germinal centers (GC).

Mef2d acts upstream to Ctla4 and down-stream to Blimp1 in regulating Treg suppressive properties. As Ctla4 (18) and Blimp1 (19) are key regulators of Tfr functions and B cell responses, we investigated whether Mef2d deletion in Foxp3+ cells would affect Tfr and Tfh responses. Similarly to Ctla4 and Blimp1, Mef2d KO showed increased Tfr and Tfh cells (Fig. 6A & B). While the total numbers of B cells, memory B cells and plasma cells were not altered (Fig. 6C), increased numbers of B1 (Fig. 6D), follicular type I B (Fig. 6E), transitional T3 B (Fig. 6H) and GC (Fig. 6I) B cells were observed in Mef2d -/- mice. The rise in follicular type I B cells and the corresponding drop in marginal zone precursors (Fig. 6F & G) observed after Mef2d depletion suggest an enhancement of BCR signals (49). The expansion of the germinal center and the alteration of BCR signaling indicate increased GC reactions. Consistent with that, moderate levels of autoantibodies were found in Mef2d-/- mice (Fig. 6J and Supplemental Fig. 5J).

Mef2d deletion dampens Treg function in vivo. As we predicted that Tregs require Mef2d to acquire the features of highly suppressive eTregs, we established three animal models to assess the effects of Mef2d deletion on Tregs *in vivo*.

First, we tested the strength of Mef2d-/- Tregs to inhibit homeostatic proliferation of CD4 and CD8 T cells over 28 days following their adoptive transfer into Rag1-/- mice (30). In comparison to WT Tregs, Mef2d-/- Tregs were severely impaired in their capability to suppress the proliferation of CD4 Teffs in the lymph nodes (Fig. 7A). In addition, upon activation they produced more IFN-γ (Fig. 7B & Supplemental Fig. 6A) and IL-2 (Fig. 7C & Supplemental Fig. 6B). No differences were observed in the spleen (Fig. 7A/F and Supplemental Fig. 6E), even though Mef2d-/- Tregs were less activated in both spleen and lymph nodes (Fig. 7D & Supplemental Fig. 6C). Increased proportions of Mef2d-/- Tregs were found among the splenocytes but not in lymph nodes (Fig. 7E and Supplemental Fig. 6D) and this was not due to altered expression of chemokine receptors (Supplemental Fig. 6F) or changes in proliferation (Supplemental Fig. 4D & E). Finally, Mef2d-/- Tregs were found to be even more strongly impaired in their ability to repress CD8 T cell proliferation and/or survival (Fig. 7G & H).

Second, we performed cardiac allografting using BALB/c donors and WT or Mef2d-/- C57BL/6 recipients in conjunction with costimulation blockade with CD40L (CD154) mAb plus donor splenocyte transfusion (DST) (49). Costimulation blockade induced long-term allograft survival (>100 d) in WT recipients but not in mice with

conditional deletion of Mef2d-/- within their Treg cells ($p<0.01$) (Fig. 7I). The acute rejection observed in Mef2d-/- mice correlated with CD8 T cell activation and intragraft expression of IFN-γ and granzyme-b (Fig. 7J) and an impairment of Tregs (Fig. 7K). Histologic examination of allografts in Mef2d-/- recipients collected just prior to end-stage rejection at 16 days post-transplant (post-Tx) showed marked differences with allografts harvested from WT recipients at the same interval post-Tx (Supplemental Fig. 7). The latter showed well preserved myocardium and vessels and small numbers of mononuclear cells palisading within capillaries and occasional interstitial areas. In contrast, allografts in Mef2d-/- mice showed widespread myocyte necrosis and vascular injury with fibro-intimal proliferation, mixed mononuclear and polymorphonuclear infiltrates and interstitial hemorrhages. Rejecting allografts also showed vascular deposition of C4d (Supplemental Fig. 8). Collectively, these findings in Mef2d-/- recipients are consistent with increased host cellular and humoral alloresponses.

Third, as shown next, we studied the effects of deletion of Mef2D in Tregs on host anti-tumor immunity.

Mef2d deletion promotes anti-tumor immunity. We used three models involving tumor growth in syngeneic mice; two lung cancer cell lines (TC1 and AE.17) were injected subcutaneously, and a hepatocellular carcinoma (HCC) cell line was delivered by injection of the mesenteric vein.

The growth of TC1 cells was profoundly impaired in Mef2d-/- mice; in 9 of 10 mice the tumors were almost completely cleared (Fig. 8A), in conjunction with activation (Fig. 8B & C) and IFN-γ production by CD4 (Fig. 8D & E) and CD8 (Fig. 8F-I) T cells in the tumor draining lymph nodes. Compared to WT tumor-bearing mice, Mef2d-/- mice had increased activation of CD4 Teffs ($CD44_{hi}CD62L_{lo}$, Fig. 8B & C) that was inversely correlated with the impairment in Treg functions (IL-10 production, Ctla-4 and Ki67 expression, Supplemental Fig. 9A-F). Moreover, Tregs harvested from the tumor draining lymph nodes evidenced transcriptome alterations (Supplemental Fig. 9G) consistent with that of Tregs in non-tumor bearing Mef2d-/- mice (Fig. 3G). The infiltration of Tregs in TC1 tumors was assessed after 8 days, so as to precede shrinking of the tumors. Mef2d-/- Tregs infiltrated the tumor as well as WT Tregs (Fig. 8K). However, tumor infiltrating CD4 and CD8 T cells were more numerous and more activated in Mef2d-/- mice (Fig. 8K & L and Supplemental Fig. 9H), likely as a consequence of impaired Treg functions (Supplemental Fig. 9A-F). The increased numbers of HPV/TC1-specific tetramer-positive CD8 T cells in Mef2d-/- mice suggest that the activation of CD8 T cells was tumor-specific

(Fig. 8J). Similarly to TC1, the growth of AE.17 tumors was impaired in Mef2d-/- mice (Fig. 8M), and again the proportions of activated and IFN-γ producing CD8 (Fig. 8N and Supplemental Fig. 9I) and CD4 (Supplemental Fig. 9J & K) T cells were increased within the draining lymph nodes.

Finally, the injection of HCC cells via the mesenteric vein, after 9 days gave rise to histologically confirmed liver tumors in 7 of 10 WT mice but in only 2 of 10 mice Mef2d-/- littermates (Fig. 9A). As the tumors differed markedly in the number and dimensions of the lesions, we used α-fetoprotein (AFP) levels in the serum as a read-out of tumor growth (50). In C57BL/6 mice, levels of serum AFP >200 ng/ml correlated with HCC growth (50). Serum AFP levels in WT mice were significantly higher than in Mef2d-/- mice or in C57BL/6 mice not injected with HCC cells (median values ± SE: C57BL/6 healthy: 60.6 ± 8.1; WT HCC: 204.5 ± 21.5; Mef2d-/- HCC: 122.3 ± 17.9) (Fig. 9B). In Mef2d-/- mice, conventional CD4 cells were more active ($CD44^{hi}/CD62L^{lo}$ and CD69+, Fig. 9C/D and Supplemental Fig. 10A/B), produced more IFN-γ (Fig. 9E & Supplemental Fig. 10C) and were more proliferative (Fig. 9F & Supplemental Fig. 10D). Conversely, the Treg population was less proliferative (Fig. 9G & Supplemental Fig. 10E) and was characterized by lower levels of Ctla-4 (Fig. 9H & Supplemental Fig. 10F) and IL-10 (Fig. 9I & Supplemental Fig. 10G). The alterations in the transcriptome (Fig. 9J) and in the proteome (Fig. 9K) typical of Mef2d-/- Tregs were maintained or became even greater in HCC-bearing mice. No significant differences were observed in the CD8 population (Supplemental Fig. 10H & I) or in the production of IL-2 by CD4 cells (Supplemental Fig. 10J). Comparable data illustrating the marked inhibitory effects of Mef2d deletion in Tregs on HCC tumor growth were seen at day 21 post-injection (Supplemental Fig. 11).

Mef2d assembles repressive and activating complexes to maintain Treg immunosuppressive properties. To gain more insight into the mechanisms elicited by Mef2d in sustaining Treg suppressive properties, we performed ChIP using freshly isolated WT and Mef2d-/- Tregs. We mapped the bindings of Mef2d with three different antibodies (specific for α1, α2 and a pan-antibody to IP both isoforms) on the more relevant genomic loci identified as being under the control of Mef2d. We mapped in the same loci Foxp3 and p300, while the comparison of H3K27ac levels between WT and Mef2d-/- Tregs provided a read-out of the positive or negative transcriptional activities of the investigated complexes. In the case of *Ctla4/Icos* we investigated seven regions that bear MEF2

binding sites and/or were previously pulled down by Foxp3 in ChIP experiments (Supplemental Fig. 12A, Fig. 10A-G). Foxp3 significantly bound the proximal promoter (region A) and an intronic region (region D) of *Ctla4* (Fig. 10A/D). We did not find significant co-association of Mef2d in these chromatin positions, while both Mef2d α1 and Mef2d α2 precipitated the intronic region C (Fig. 10C). A decrease in H3K27ac levels in Mef2d-/- Tregs was observed in the proximal promoter (region A) and in the intronic region C (Fig. 10A/C); in these positions a significant drop in p300 binding was observed (Fig. 10A/C). Mef2d (pan and Mef2d α2 isoform) and Foxp3 were co-associated at the *Icos* promoter (region G); this region was characterized by decreased H3K27ac in Mef2d-/- cells (Fig. 10G), while a drop in p300 binding was also observed at the distal promoter (region F, Fig. 10F). Mef2d was previously described as a positive regulator of *Il10* transcription in T cells (51, 52) and in glial cells (53), through direct binding to the proximal promoter (53). We confirmed binding of Mef2d (α1, α2 and pan) to the proximal promoter of *Il10*, in association to p300 but in the absence of Foxp3 (Fig. 10H). In Mef2d-/- Tregs, decreased levels of p300 binding and H3K27ac were observed (Fig. 10H). Mef2d was associated with the *Nr4a1* promoter (Fig. 10I), as observed in other contexts (29, 54-57); the same region is bound by Foxp3 (Fig. 10I) and p300. In this locus, Mef2d appeared to form a repressive complex, as the KO had increased p300 binding and H3K27ac (Fig. 10I). Mef2d was found to be significantly associated to *Hdac9* promoter (Fig. 10J), used as a positive control. Finally, Mef2d also repressed the transcription of *Itk*, without perturbing p300 binding but inducing H3K27 deacetylation at the promoter level, probably by promoting the engagement of Foxp3 (Fig. 10K). Among the genes bound and regulated by Mef2d in Tregs, some (*Hdac9* and *Il10*) were also under Mef2d control in Teffs (Fig. 10L and Supplemental Fig. 12B & C), as well as in non-lymphoid organs and cell-types (24, 34, 38, 52, 54, 56). Others, like *Icos* and *Ctla4*, were Tregs restricted, probably because Mef2d binding requires the establishment of a permissive open chromatin status (Fig. 10L and Supplemental Fig. 12B & C), primed by Foxp3.

In summary, Mef2d established both repressive and activating complexes on relevant loci for Tregs homeostasis and immune suppressive functions. In some cases, its binding was directly assisted by Foxp3 (*Icos* promoter region G and *Nr4a1*); in a second group of loci (*Ctla4* region C) Mef2d assisted the transcription proficiency stimulated by Foxp3, while in others the Mef2d transcriptional effect was Foxp3-independent (*Il10* and *Hdac9*). The activating or repressive functions of Mef2d depend on the co-repressors or co-activators

recruited to chromatin. We observed perfect correlation between H3K27ac, p300 and the transcriptional activity in all the examined loci, except for *Itk*, which appeared to be regulated through an indirect mechanism.

Discussion

MEF2 transcription factors regulate differentiative and adaptive/stress-related responses (22). In mammals, MEF2D is the most ubiquitously expressed of the 4 paralogs, being abundant in almost all tissues and cell types (22). This wide expression pattern reflects the key roles of MEF2D in regulating general responses involved in maintaining cellular fitness, including the control of cell-cycle progression, mitochondrial activity and the balance of pro-survival and apoptotic responses (22, 41). However, MEF2D also has tissue/cell-type specific functions, like the promotion of muscle differentiation, remodeling, regeneration and the control of neuronal development and synaptogenesis (22, 41). Moreover, MEF2D controls the development of particular cell types, like retina photoreceptors (58). Three mechanisms allow MEF2D to exert context-dependent biological functions: i) the plasticity of MEF2D containing complexes and the co-existence in the same cell of MEF2 transcriptional activator and repressor complexes (38); ii) the ability to bind chromatin away from its traditional consensus sites thanks to MEF2 binding to lineage-specific transcription factors (58); and iii) the expression of cell-specific MEF2 isoforms that display differential affinity for cofactors (33, 36).

We found that all three of these mechanisms are operative in Tregs. The expression of Foxp3 triggers the alternative splicing mechanism that gives rise to the α2 isoform of Mef2d. This isoform is refractory to the binding to class IIa HDACs and HDAC9, in particular, and has higher affinity for Foxp3. The α1 isoform retains a reduced capability to interact with Foxp3 and a stronger affinity for HDACs. The co-presence of the two isoforms sustains the expression of Treg specific genes, maintaining the balance between the establishment of activating and repressive transcriptional complexes. We observed that in Tregs, Mef2d and Foxp3 can act synergistically (on *Icos* and *Nr4a1* loci), additively (on *Ctla4* and *Il10*), or independently (on *Itk* and *Hdac9*). A fine regulation of this balance ensures the maintenance of the highly suppressive properties of Tregs. In particular Mef2d-/- Tregs fail to generate eTreg cells. Mef2d appears to be downstream of Blimp1, the main regulator of IL-10+ eTregs (21), as the core of Blimp1 regulated genes (47) show evidence of MEF2 binding at their promoters. Moreover, as Blimp1 directly controls only 8% of the eTreg signature (59), we can now identify Mef2d among the transcription factors involved in sustaining the eTreg phenotype.

In fact, while Mef2d-/- Tregs were only slightly impaired in their suppressive functions *in vitro*, they were severely impaired in repressing the proliferation of CD4 and CD8 T cells *in vivo*. Moreover, the activation of CD4 and CD8 T cells after the depletion of *Mef2d* in Tregs induced allograft rejection and promoted anti-tumor immunity, as seen in three different cancer models (HCC and lung) known for being Treg-dependent *in vivo* (60-62). Interestingly, in HCC and in NSCLC, as in various tumors, MEF2D expression is increased and reported to be required to sustain tumor growth (63-65). The up-regulation of PD-L1 frequently observed in HCC has been correlated to the impairment of CD8-mediated cytotoxicity (66) and could explain the inefficient activation of CD8 lymphocytes observed in this model in Mef2d-/- mice. As Mef2d was found to control the expression of PD-L1 (67), in these cancers a targeted therapy to inhibit MEF2D functions could have a double benefit of decreasing the malignancy of tumor cells and increasing the immunoreactivity of T cells. Regarding this, small molecules that target the interaction of Mef2 with class IIa Hdacs have been reported (65, 66).

The lack of signs of severe inflammation or autoimmunity in mice depleted of *Mef2d -/-* in Foxp3+ Tregs is in line with the effects of deletion of *Blimp1* (45), *Icos* (67) and *Il10* (68). In the latter, no autoimmunity but mild colitis was reported (68), while *Prdm1 -/-* mice display marks of autoimmunity only in aging mice (59). Moreover, similarly to Mef2d, the ablation of *Blimp1*, *Icos*, *Il10* or *Ctla4* in Tregs does not impact their suppressive properties *in vitro*, but impairs their activation under stimulating conditions (48) (Fig. 5I-J) and their activities *in vivo* (45, 67-70), similarly to our Mef2d-/- mice. Mef2d functions in Tregs are not limited to the maintenance of a suppressive phenotype, as the proliferation of Mef2d-/- Tregs was also impaired, similarly to *Icos*-/- Tregs (71). Moreover, there is indirect evidence of the involvement of Mef2d in the regulation of Treg metabolism (31). Finally, and again similarly to Ctla4 (18) and Blimp1 (19), the depletion of Mef2d in Foxp3+ cells affects Tfr functions and impacts the normal maturation of B lymphocytes and the development of GC reactions. As a result of these alterations (50), Mef2d-/- mice accumulate small quantities of autoantibodies, though not sufficient to induce significant autoimmunity. It is currently unknown whether the unbalanced B-cell homeostasis observed in Mef2d -/- mice may actively contribute to anti-cancer immunity. Further studies are required to clarify this point.

There are no reports in the literature regarding the association of autoimmunity and MEF2D copy-number loss or genetic deletion, probably because of MEF2D pleiotropy. However, a rare SNP that abrogates the

expression of the α2 isoform of MEF2D was recently associated with systemic lupus erythematosus (72), and SNPs associated with multiple sclerosis at the level of enhancer and super-enhancers were predicted to alter the binding of MEF2 transcription factors (73). Further investigations are required to unveil a likely direct role played by MEF2 transcription factors in these diseases, given our discoveries in Tregs. Finally, our work underlines the importance played by MEF2D in the regulation of anti-cancer immunity, offering an alternative interpretation to the conflicting evidence about the contribution of MEF2D to oncogenesis (41).

Methods

Mice. We used BALB/c, Rag1$^{-/-}$ C57BL/6 and CD90.1/B6 mice from The Jackson Laboratory, plus previously described Foxp3$^{YFP\text{-}cre}$ mice (68) and Mef2d$^{flox/flox}$ mice (40) that were backcrossed on the C57BL/6 background at least 8 times and used at 6–8 weeks of age, unless specified. *Foxp3$^{YFP\text{-}cre}$* mice were used as wild-type controls.

Plasmids and transfections. We purchased Mef2d-FLAG-MYC plasmids from Origene and FLAG-tagged Foxp3 from Addgene. Mef2d-GFP and MEF2D deletion mutants were previously described (38). Hdac9-FLAG was obtained from Dr. Ed Seto (George Washington University, Washington, DC) (74). Mef2dα1 and Mef2dα2 were obtained from Dr. F. Jeffrey Dilworth (Ottawa Hospital Research Institute, Ottawa, Canada) (36). HEK-293T cells were grown in DMEM plus 10% FBS and transfected with Lipofectamine 2000 (Invitrogen #11668027).

Co-immunoprecipitation (Co-IP) and Western blotting. HEK-293T, Teff and Treg cells were lysed with a hypotonic buffer (20 mM Tris-HCl, pH 7.5; 2 mM EDTA; 10 mM $MgCl_2$; 10 mM KCl; and 1% Triton X-100) supplemented with protease inhibitors. For each immunoprecipitation, 1 μg of antibody was used. Ab-antigen complexes were collected with Protein-G agarose (Invitrogen, #15920-010). Cell lysates were separated by SDS-PAGE, transferred to nitrocellulose membranes and immunoblotted with the following Abs: Mef2d (BD, #610774), Foxp3 (Invitrogen, #700914, eBioscience, #14-4774-82, #13-5773-80), p300 (Invitrogen, #PA1-848), Flag (Cell Signaling Technology, #14793), Myc (CST, #2272), HA (CST, #2367), phospho-Histone H2A.X (Ser139, CST, #9718), Histone H2A.X (CST, #7631), p53 mAb (DO-1, CST, #18032), β-actin (CST, #3700), Blimp1 (eBioscience, 6D3, #14-5963-82), Hdac3 (Abcam, #ab7030), Crabp2 (Santa Cruz Biotechnology, #sc-166897), Fabp5 (SC, #sc-365236), Lmnb1 (SC, # sc-377000), Ki67 (Abcam, # ab15580), p53 ac (K120) (Abcam, #78316), and Mef2d (α1 and α2)(36). Secondary HRP-conjugated Abs to mouse (#7076), rat (#7077) and rabbit (#7074) IgG were purchased from CST. Unconjugated CD3 (clone 145-2C11, #553057) and CD28 (clone 37.51, #553294) mAbs used for cell activation were purchased from BD.

Cryopreservation. Single cell suspensions in CryoStor CS5 cryopreservation media (Sigma-Aldrich) reagent were frozen in -80°C, stored in liquid nitrogen, then thawed and transferred quickly into warm TCM (> 10x volume) for use. Cell number and viability were assessed with a Nexcelom Cellometer Auto2000 and AOPI Staining solution in PBS.

Flow cytometry. Single-cell suspensions from lymph nodes, spleens or tumors were prepared as previously described (75) and were stained with fluorochrome-conjugated mAbs from BD Biosciences, unless specified otherwise, that were directed against CD4 (Pacific blue, Invitrogen, #MHCD0428), CD8 (Super Bright 645, eBioscience, clone 53-6.7,#64-0081-82), Foxp3 (eFluor 450, eBioscience, clone FJK-16s, #48-5773-82 and PE-Cy5 #15-5773-82), CD62L (PE-Cy7, clone MEL-14, #25-0621-82), IFN-γ (APC, clone XMG1.2, #554413; PE # 554412), CD44 (PE-Cyaine5, eBioscience, clone IM7, #15-0441-83), Ctla4 (APC, #17-1522-82), Icos (PE, # 12-9949-81), Ki67 (APC700, #561277), IL-2 (PE, eBioscience, clone JES6-5H4, # 12-7021-41), CD25 (APC, eBioscience, clone PC61.5, #17-0251-82), CD8a (FITC, #53-6.7), CD4 (FITC, #H129.19), NK1.1 (FITC, #M1/70 BioLegend), CD11b (FITC, #M1/70 BioLegend), CD19 (BV605, #6D5 BioLegend), CD45R/B220 (BV785, #RA3-6B2 BioLegend), IgM (PerCP-Cy5.5, #II-41, Invitrogen), CD62L (PE, #MEL-14, BioLegend), CD95 (PE-CF594, #Jo2), GL7 (APC, #GL7, BioLegend), CD138 (APC-R700, #281-2), CD93 (PE/Cy7, #AA4.1, BioLegend), CD23 (APC Cy7, #B3B4, BioLegend), CD21/35 (PB, #7E9, BioLegend), CD19 (FITC, #6D5, BioLegend), CD4 (PE-CF594, # RM4-5), CXCR5 (APC, #L138D7, BioLegend), PD-1 (PE/Cy7, #29F.1A12, BioLegend), Foxp3 (PB, #FJK-16s, Invitrogen) and acquired on a Cytoflex (Beckman Coulter) flow cytometer.

Treg suppression assays. For *in vitro* studies, $5\times10_4$ $CD4^+CD25^-$ T/YFP- cells and $CD4^+CD25^+$/ YFP+ Tregs from $Foxp3^{YFP\text{-}Cre}$ and $Mef2d^{-/-}$mice isolated using $CD4^+CD25^+$Treg isolation kit (Miltenyi Biotec, #130-091-041) or cell sorted were added to 96-well plates. Equal numbers of CFSE-labeled $CD4^+CD25^-$ T cells and γ-irradiated antigen-presenting cells (APC), isolated using a CD90.1 kit (Miltenyi Biotec, #130-049-101), plus CD3 mAb (1 μg/ml), were cultured for 72 h. After 72 h, proliferation of Teff cells was determined by flow and analysis of cell trace violet dilution. The same assay was performed by using Tregs isolated from mice treated with IL-2/anti-IL-2 complexes (76), or by pre-activating Tregs for 2 days with CD3/CD28 beads (1:1) and IL-2 (10 U/ml)(48). For Treg assay performed by using WT splenocytes as responder cells, WT splenocytes were CFSE-labeled and

cultured in the presence of WT and Mef2d-/- Tregs for three days under CD3 stimulation (CD3mAb, 1 μg/ml).

For *in vivo* homeostatic proliferation assay, $0.2\times10_6$ $CD4_+CD25_-$ Thy1.1+ or $0.2\times10_6$ CD8+Thy1.1+ and $1.0\times10_6$ Tregs were injected via the tail vein into $Rag1_{-/-}$ mice. At 1 or 4 weeks later, lymph node and spleens were harvested and stained with Thy1.1-PE and CD4-Pacific blue or CD8-Super Bright 645, and the numbers of $Thy1.1_+$ T cell cells determined using a Cytoflex flow cytometer.

Cardiac transplantation. Heterotopic cardiac allografts were performed using BALB/c donors and WT or Mef2d-/- recipients on the C57BL/6 background (77). At the time of engraftment, recipients were treated i.v. with CD154 mAb (200 μg) plus $5\times10_6$ donor splenocytes (49). Allograft survival was monitored by palpation of ventricular contractions and confirmed by histological evaluation.

Detection of autoantibodies. Sera of three WT and Mef2d-/- mice were tested for autoantibodies by indirect immunofluorescence. Non-fixed 4-5 uM cryosections of WT tissues were incubated for 1h at RT with serial dilutions (from 1:1 up to 1:80) of sera, washed in PBS, and incubated for 30' at RT with FITC-labeled goat anti-mouse secondary antibody (Jackson Immunoresearch Lab, # 115-545-062, diluted in PBS, 1:200). After washings in PBS, slides were mounted and evaluated by specialist in autoimmune clinical diagnostics in human autoimmune diseases. Pre-characterized sera from mice with known autoantibodies of corresponding specificity were used as positive controls, while pooled sera from WT B6 mice and secondary antibodies only were used as negative controls. All positive sera were analyzed a second time to evaluate individual titers.

Immunoperoxidase. Formalin-fixed, paraffin-embedded sections of allografts harvested at 14 days post-Tx were stained by immunoperoxidase with rabbit antibodies directed against CD3 (#A0452, Agilent), C4d (#12-5000, American Research Products) or rabbit IgG control antibody (#I-1000, Vector Labs) (49).

ChIP assays. Teffs or Tregs were fixed for 15' with 1% formaldehyde and fragmented by sonication. Chromatin was immunoprecipitated as previously described (38) using Abs against H3K27ac (2μg, Abcam #ab4729), Mef2d (5 μg, BD, # 610774), Mef2d α1 and α2 (36) (5 μg), p300 (3μg, Invitrogen #PA1-848) and Foxp3 (10 μg, Invitrogen # PA1-806). The immunoprecipitated DNA was purified and analyzed by qPCR (SYBR green, Applied Biosystems).

RNA-seq and real-time qPCR. RNA was isolated using RNeasy kits (QIAGEN), and RNA integrity and quantity were analyzed by NanoDrop ND-1000 and Nanochip 2100 Bioanalyzer (Agilent Technologies). Library preparation and RNA sequencing, genome mapping and analysis were performed by Novogene (Sacramento, CA) on the Illumina Platform PE150; data were deposited at the NCBI GEO site (accession GSE139480). The edgeR package was used to identify the differentially expressed genes (p-value <0.05 and fold change >1.3). GSEA(78) was performed to identify altered signaling pathways, as previously described (38). Expression of individual genes was verified by qPCR. RNA was reverse transcribed to cDNA (Applied Biosystems) and RT-qPCR was performed using Taqman primer and probe sets; data were normalized to endogenous 18s rRNA, and relative expression was determined by the formula $2^{-\Delta CT}$.

Cell lines and tumor models. The murine lung adenocarcinoma cells, TC1 (79), were provided by Dr. Yvonne Paterson (UPenn, Philadelphia, PA). The murine AE17.ova mesothelioma cell line (80) was provided by Dr. Delia Nelson, University of Western Australia, Perth, Australia. The murine HCC cell line, Dt81-Hepa1-6, was developed by Dr. Marc Bilodeau (Centre Hospitalier de l'Université de Montréal, Montreal, Canada) (81). Lung cancer cells were grown in RPMI, HCC in DMEM/F-12 supplemented with 10% fetal bovine serum (FBS), 2 mM glutamine, and 5 μg/ml penicillin & streptomycin. For lung tumor cells, each mouse was shaved on their right flank and injected s.c. with 1.2×10^6 TC1 or 2×10^6 AE17 tumor cells, whereas HCC $0.3\text{x}10^6$ cells were injected directly into the mesenteric vein. Tumor volume was determined by the formula: $V = (W^2 \times L)/2$. Serum AFP was measured by using mouse alpha-fetoprotein/AFP Quantikine ELISA Kit (MAFP00, R&D Systems).

Statistics. Data were analyzed using GraphPad Prism 8.0. Data are presented as mean ± SD unless specified otherwise. Measurements between two groups were done with a 2-tailed Student's t test if data were normally distributed or Mann-Whitney U unpaired test when the populations were not normally distributed. Comparison of multiple samples were performed by 1-way ANOVA with corresponding Tukey's multiple comparison test. Graft survival was evaluated with Kaplan-Meier followed by log-rank test. AUC for suppression assays was calculated as previously described (83); AUC for KO samples were expressed as ratio to WT, then ratios of 3 experiments were combined and tested for significance (one-sample T test with theoretical mean = 1). We marked

with *p<0.05, **p<0.01, ***p<0.005.

Study approval. Animal studies were approved by the Institutional Animal Care and Use Committee of the Children's Hospital of Philadelphia (protocols 17-001047 and 19-000561).

Primers. We used the primers listed in Table 2.

Author contributions

EDG designed and performed experiments, analyzed data and drafted the manuscript. LW performed cardiac allografts, performed experiments, and analyzed data. YX performed experiments and analyzed data. TA performed experiments and analyzed data. LMC performed experiments and analyzed data. RH provided technical assistance. AB performed experiments. TRB performed experiments. MT provided technical support. UHB provided assistance with RNA-seq studies. WWH oversaw experimental design and writing of the manuscript.

Acknowledgments

This work was supported by NIH grants R01 AI12324 and R01 CA177852 (to W.W. Hancock). E.D.G received a “Fondazione Umberto Veronesi Fellowship”. Specified plasmids were purchased from Addgene. We acknowledge the kind gifts of reagents and cells from Dr. F. Jeffrey Dilworth (Ottawa, Canada) and from Dr. Marc Bilodeau (Montreal, Canada), respectively.

References

1. Sakaguchi S, Miyara M, Costantino CM, and Hafler DA. FOXP3+ regulatory T cells in the human immune system. *Nat Rev Immunol.* 2010;10(7):490-500.

2. Tanaka A, and Sakaguchi S. Regulatory T cells in cancer immunotherapy. *Cell Res.* 2017;27(1):109-18.

3. Rudensky AY. Regulatory T cells and Foxp3. *Immunol Rev.* 2011;241(1):260-8.

4. Samstein RM, et al. Foxp3 exploits a pre-existent enhancer landscape for regulatory T cell lineage specification. *Cell.* 2012;151(1):153-66.

5. Chorro L, et al. Interleukin 2 modulates thymic-derived regulatory T cell epigenetic landscape. *Nat Commun.* 2018;9(1):5368.

6. Ren J, et al. Foxp1 is critical for the maintenance of regulatory T-cell homeostasis and suppressive function. *PLoS Biol.* 2019;17(5):e3000270.

7. Li B, et al. FOXP3 is a homo-oligomer and a component of a supramolecular regulatory complex disabled in the human XLAAD/IPEX autoimmune disease. *Int Immunol.* 2007;19(7):825-35.

8. van Loosdregt J, et al. Regulation of Treg functionality by acetylation-mediated Foxp3 protein stabilization. *Blood.* 2010;115(5):965-74.

9. Beier UH, et al. Sirtuin-1 targeting promotes Foxp3+ T-regulatory cell function and prolongs allograft survival. *Mol Cell Biol.* 2011;31(5):1022-9.

10. Huang C, et al. Cutting Edge: a novel, human-specific interacting protein couples FOXP3 to a chromatin-remodeling complex that contains KAP1/TRIM28. *J Immunol.* 2013;190(9):4470-3.

11. Wang L, et al. Histone/protein deacetylase inhibitor therapy for enhancement of Foxp3+ T-regulatory cell function posttransplantation. *Am J Transplant.* 2018;18(7):1596-603.

12. Tanaka S, Pfleger C, Lai JF, Roan F, Sun SC, and Ziegler SF. KAP1 regulates regulatory T cell function and proliferation in both Foxp3-dependent and -independent manners. *Cell Rep.* 2018;23(3):796-807.

13. Huang J, et al. Histone/protein deacetylase 11 targeting promotes Foxp3+ Treg function. *Sci Rep.* 2017;7(1):8626.

14. Lee S, Park K, Kim J, Min H, and Seong RH. Foxp3 expression in induced regulatory T cells is stabilized by C/EBP in inflammatory environments. *EMBO Rep.* 2018;19(12).

15. Carpenter AC, et al. Control of regulatory T cell differentiation by the transcription factors Thpok and LRF. *J Immunol.* 2017;199(5):1716-28.

16. Ohnmacht C, et al. The microbiota regulates type 2 immunity through RORgamma(+) T cells. *Science.* 2015;349(6251):989-93.

17. Sefik E, et al. Individual intestinal symbionts induce a distinct population of RORgamma(+) regulatory T cells. *Science.* 2015;349(6251):993-7.

18. Chung Y, et al. Follicular regulatory T cells expressing Foxp3 and Bcl-6 suppress germinal center reactions. *Nat Med.* 2011;17(8):983-8.

19. Linterman MA, et al. Foxp3+ follicular regulatory T cells control the germinal center response. *Nat Med.* 2011;17(8):975-82.

20. Fang D, and Zhu J. Dynamic balance between master transcription factors determines the fates and functions of CD4 T cell and innate lymphoid cell subsets. *J Exp Med.* 2017;214(7):1861-76.

21. Cretney E, et al. The transcription factors Blimp-1 and IRF4 jointly control the differentiation and function of effector regulatory T cells. *Nat Immunol.* 2011;12(4):304-11.

22. Potthoff MJ, and Olson EN. MEF2: a central regulator of diverse developmental programs. *Development.* 2007;134(23):4131-40.

23. Ma K, Chan JK, Zhu G, and Wu Z. Myocyte enhancer factor 2 acetylation by p300 enhances its DNA binding activity, transcriptional activity, and myogenic differentiation. *Mol Cell Biol.* 2005;25(9):3575-82.

24. Miska EA, Karlsson C, Langley E, Nielsen SJ, Pines J, and Kouzarides T. HDAC4 deacetylase associates with and represses the MEF2 transcription factor. *EMBO J.* 1999;18(18):5099-107.

25. Swanson BJ, Jack HM, and Lyons GE. Characterization of myocyte enhancer factor 2 (MEF2) expression in B and T cells: MEF2C is a B cell-restricted transcription factor in lymphocytes. *Mol Immunol.* 1998;35(8):445-58.

26. Pan F, Ye Z, Cheng L, and Liu JO. Myocyte enhancer factor 2 mediates calcium-dependent transcription of the interleukin-2 gene in T lymphocytes: a calcium signaling module that is distinct from but collaborates with the nuclear factor of activated T cells (NFAT). *J Biol Chem.* 2004;279(15):14477-80.

27. Matsuoka H, et al. Disruption of HDAC4/N-CoR complex by histone deacetylase inhibitors leads to inhibition of IL-2 gene expression. *Biochem Pharmacol.* 2007;74(3):465-76.

28. Esau C, Boes M, Youn HD, Tatterson L, Liu JO, and Chen J. Deletion of calcineurin and myocyte enhancer factor 2 (MEF2) binding domain of Cabin1 results in enhanced cytokine gene expression in T cells. *J Exp Med.* 2001;194(10):1449-59.

29. Dequiedt F, et al. HDAC7, a thymus-specific class II histone deacetylase, regulates Nur77 transcription and TCR-mediated apoptosis. *Immunity.* 2003;18(5):687-98.

30. Tao R, et al. Deacetylase inhibition promotes the generation and function of regulatory T cells. *Nat Med.* 2007;13(11):1299-307.

31. Beier UH, et al. Essential role of mitochondrial energy metabolism in Foxp3(+) T-regulatory cell function and allograft survival. *FASEB J.* 2015;29(6):2315-26.

32. Kasler HG, Lim HW, Mottet D, Collins AM, Lee IS, and Verdin E. Nuclear export of histone deacetylase 7 during thymic selection is required for immune self-tolerance. *EMBO J.* 2012;31(23):4453-65.

33. Hakim NH, Kounishi T, Alam AH, Tsukahara T, and Suzuki H. Alternative splicing of Mef2c promoted by Fox-1 during neural differentiation in P19 cells. *Genes Cells.* 2010;15(3):255-67.

34. Di Giorgio E, Gagliostro E, Clocchiatti A, and Brancolini C. The control operated by the cell cycle machinery on MEF2 stability contributes to the downregulation of CDKN1A and entry into S phase. *Mol Cell Biol.* 2015;35(9):1633-47.

35. Martin JF, Miano JM, Hustad CM, Copeland NG, Jenkins NA, and Olson EN. A Mef2 gene that generates a muscle-specific isoform via alternative mRNA splicing. *Mol Cell Biol.* 1994;14(3):1647-56.

36. Sebastian S, et al. Tissue-specific splicing of a ubiquitously expressed transcription factor is essential for muscle differentiation. *Genes Dev.* 2013;27(11):1247-59.

37. Gao C, et al. RBFox1-mediated RNA splicing regulates cardiac hypertrophy and heart failure. *J Clin Invest.* 2016;126(1):195-206.

38. Di Giorgio E, et al. The co-existence of transcriptional activator and transcriptional repressor MEF2 complexes influences tumor aggressiveness. *PLoS Genet.* 2017;13(4):e1006752.

39. Rudra D, et al. Transcription factor Foxp3 and its protein partners form a complex regulatory network. *Nat Immunol.* 2012;13(10):1010-9.

40. Kim Y, et al. The MEF2D transcription factor mediates stress-dependent cardiac remodeling in mice. *J Clin Invest.* 2008;118(1):124-32.

41. Di Giorgio E, Hancock WW, and Brancolini C. MEF2 and the tumorigenic process, hic sunt leones. *Biochim Biophys Acta Rev Cancer.* 2018;1870(2):261-73.

42. Fu W, et al. A multiply redundant genetic switch 'locks in' the transcriptional signature of regulatory T cells. *Nat Immunol.* 2012;13(10):972-80.

43. Cretney E, Kallies A, and Nutt SL. Differentiation and function of Foxp3(+) effector regulatory T cells. *Trends Immunol.* 2013;34(2):74-80.

44. Zheng Y, et al. Regulatory T-cell suppressor program co-opts transcription factor IRF4 to control TH2 responses. *Nature.* 2009;458(7236):351-6.

45. Bankoti R, et al. Differential regulation of effector and regulatory T cell function by Blimp1. *Sci Rep.* 2017;7(1):12078.

46. Yu J, Angelin-Duclos C, Greenwood J, Liao J, and Calame K. Transcriptional repression by blimp-1 (PRDI-BF1) involves recruitment of histone deacetylase. *Mol Cell Biol.* 2000;20(7):2592-603.

47. Wei X, et al. Reciprocal expression of IL-35 and IL-10 defines two distinct effector Treg subsets that are required for maintenance of immune tolerance. *Cell Rep.* 2017;21(7):1853-69.

48. Koizumi SI, et al. JunB regulates homeostasis and suppressive functions of effector regulatory T cells. *Nat Commun.* 2018;9(1):5344.

49. Hancock WW, Sayegh MH, Zheng XG, Peach R, Linsley PS, and Turka LA. Costimulatory function and expression of CD40 ligand, CD80, and CD86 in vascularized murine cardiac allograft rejection. *Proc Natl Acad Sci U S A.* 1996;93(24):13967-72.

50. Princler GL, Vlahakis G, Kortright KH, Okada S, and McIntire KR. Dynamics of serum alpha-fetoprotein during spontaneous hepatocellular carcinoma development in mice. *Eur J Cancer Clin Oncol.* 1981;17(12):1241-8.

51. Liopeta K, et al. cAMP regulates IL-10 production by normal human T lymphocytes at multiple levels: a potential role for MEF2. *Mol Immunol.* 2009;46(3):345-54.

52. Boubali S, et al. Calcium/calmodulin-dependent protein kinase II regulates IL-10 production by human T lymphocytes: a distinct target in the calcium dependent pathway. *Mol Immunol.* 2012;52(2):51-60.

53. Yang S, et al. Transcription factor myocyte enhancer factor 2D regulates interleukin-10 production in microglia to protect neuronal cells from inflammation-induced death. *J Neuroinflamm.* 2015;12:33.

54. Youn HD, and Liu JO. Cabin1 represses MEF2-dependent Nur77 expression and T cell apoptosis by controlling association of histone deacetylases and acetylases with MEF2. *Immunity.* 2000;13(1):85-94.

55. Daems C, Martin LJ, Brousseau C, and Tremblay JJ. MEF2 is restricted to the male gonad and regulates expression of the orphan nuclear receptor NR4A1. *Mol Endocrinol.* 2014;28(6):886-98.

56. Di Giorgio E, et al. MEF2 is a converging hub for histone deacetylase 4 and phosphatidylinositol 3-kinase/Akt-induced transformation. *Mol Cell Biol.* 2013;33(22):4473-91.

57. Rastogi B, Raut SK, Panda NK, Rattan V, Radotra BD, and Khullar M. Overexpression of HDAC9 promotes oral squamous cell carcinoma growth, regulates cell cycle progression, and inhibits apoptosis. *Mol Cell Biochem.* 2016;415(1-2):183-96.

58. Andzelm MM, et al. MEF2D drives photoreceptor development through a genome-wide competition for tissue-specific enhancers. *Neuron.* 2015;86(1):247-63.

59. Cretney E, et al. Characterization of Blimp-1 function in effector regulatory T cells. *J Autoimmun.* 2018;91:73-82.

60. Pedroza-Gonzalez A, et al. Activated tumor-infiltrating CD4+ regulatory T cells restrain antitumor immunity in patients with primary or metastatic liver cancer. *Hepatology.* 2013;57(1):183-94.

61. Liu Y, et al. Inhibition of p300 impairs Foxp3+ T regulatory cell function and promotes antitumor immunity. *Nat Med.* 2013;19(9):1173-7.

62. Wang L, et al. Ubiquitin-specific protease-7 inhibition impairs Tip60-dependent Foxp3+ T-regulatory cell function and promotes antitumor immunity. *EBioMedicine.* 2016;13:99-112.

63. Ma L, et al. Overexpression of the transcription factor MEF2D in hepatocellular carcinoma sustains malignant character by suppressing G2-M transition genes. *Cancer Res.* 2014;74(5):1452-62.

64. Song L, et al. miR-218 suppressed the growth of lung carcinoma by reducing MEF2D expression. *Tumour Biol.* 2016;37(3):2891-900.

65. Jayathilaka N, et al. Inhibition of the function of class IIa HDACs by blocking their interaction with MEF2. *Nucleic Acids Res.* 2012;40(12):5378-88.

66. Wei J, et al. Reversal of pathological cardiac hypertrophy via the MEF2-coregulator interface. *JCI Insight.* 2017;2(17):e91068.

67. Guo F, Iclozan C, Suh WK, Anasetti C, and Yu XZ. CD28 controls differentiation of regulatory T cells from naive CD4 T cells. *J Immunol.* 2008;181(4):2285-91.

68. Rubtsov YP, et al. Regulatory T cell-derived interleukin-10 limits inflammation at environmental interfaces. *Immunity.* 2008;28(4):546-58.

69. Sojka DK, Hughson A, and Fowell DJ. CTLA-4 is required by CD4+CD25+ Treg to control CD4+ T-cell lymphopenia-induced proliferation. *Eur J Immunol.* 2009;39(6):1544-51.

70. Paterson AM, et al. Deletion of CTLA-4 on regulatory T cells during adulthood leads to resistance to autoimmunity. *J Exp Med.* 2015;212(10):1603-21.

71. Kornete M, Sgouroudis E, and Piccirillo CA. ICOS-dependent homeostasis and function of Foxp3+ regulatory T cells in islets of nonobese diabetic mice. *J Immunol.* 2012;188(3):1064-74.

72. Farias FHG, et al. A rare regulatory variant in the MEF2D gene affects gene regulation and splicing and is associated with a SLE sub-phenotype in Swedish cohorts. *Eur J Hum Genet.* 2019;27(3):432-41.

73. Farh KK, et al. Genetic and epigenetic fine mapping of causal autoimmune disease variants. *Nature.* 2015;518(7539):337-43.

74. Yuan Z, Peng L, Radhakrishnan R, and Seto E. Histone deacetylase 9 (HDAC9) regulates the functions of the ATDC (TRIM29) protein. *J Biol Chem.* 2010;285:39329-38.

75. Kalin JH, et al. Targeting the CoREST complex with dual histone deacetylase and demethylase inhibitors. *Nat Commun.* 2018;9(1):53.

76. Boyman O, Kovar M, Rubinstein MP, Surh CD, and Sprent J. Selective stimulation of T cell subsets with antibody-cytokine immune complexes. *Science.* 2006;311(5769):1924-7.

77. Wang L, et al. FOXP3+ regulatory T cell development and function require histone/protein deacetylase 3. *J Clin Invest.* 2015;125(3):1111-23.

78. Subramanian A, et al. Gene set enrichment analysis: a knowledge-based approach for interpreting genome-wide expression profiles. *Proc Natl Acad Sci U S A.* 2005;102(43):15545-50.

79. Lin KY, et al. Treatment of established tumors with a novel vaccine that enhances major histocompatibility class II presentation of tumor antigen. *Cancer Res.* 1996;56(1):21-6.

80. Jackaman C, et al. IL-2 intratumoral immunotherapy enhances CD8+ T cells that mediate destruction of tumor cells and tumor-associated vasculature: a novel mechanism for IL-2. *J Immunol.* 2003;171(10):5051-63.

81. Lacoste B, Raymond VA, Cassim S, Lapierre P, and Bilodeau M. Highly tumorigenic hepatocellular carcinoma cell line with cancer stem cell-like properties. *PLoS One.* 2017;12(2):e0171215.

82. Niedzielska M, et al. Differential gene expression in human tissue resident regulatory T cells from lung, colon, and blood. *Oncotarget.* 2018;9(90):36166-84.

Table 1. Top10 transcription factors (TF) binding BLIMP1 regulated genes. z-scores and p-values were retrieved from BART (http://faculty.virginia.edu/zanglab/bart/) and refer to the ChIP-seq data deposited in ENCODE.

TF	z-score	p-value
NFKB	1.76	0.003
STAT5	1.67	0.001
POU2F2	1.67	0.009
BATF3	1.66	0.005
RUNX3	1.66	0.028
PAX5	1.61	0.001
MEF2	1.61	0.003
FOXP1	1.59	0.004
TBX21	1.59	0.005
BCLAF1	1.56	0.008

Table 2. Primers used in this study

PRIMER NAME	SEQUENCE 5'->3'
ITK_+34_FW	GTGCGACTGAAGGAGAGGAG
ITK_-107_RV	CATCAGAGGAGGGAGCTCAG
NR4A1_-357_FW	CCTCCTCCTGGTCGGTTATT
NR4A1_-219_RV	GCGCGGATTGTTTGATCTAT
HDAC9_-482_FW	CTCCAGAGGGTGTCCTCCTA
HDAC9_-710_RV	GGCTTTGGTGGGGTATTTTT
CTLA4_+4397_FW	AAGGAGCAGGAAGGATAGGG
CTLA4_+4584_RV	GCTGCTCCATGTTGTTCAAA
CTLA4_+4003_FW	CTTGTCCCTTTGATGGCACT
CTLA4_+4200_RV	TGGATCTGCAACAGAAGACG
CTLA4_-210_FW	CTCCAAGACTCCACGTCTCC
CTLA4_+15_RV	AGCCGTGGGTTTAGCTGTTA
CTLA4_+1959_FW	CCCGCTAAGCTGATGGAGTA
CTLA4_+2199_RV	TACCCCAGGCTTAGTTTCCA
CTLA4_+6339_FW	AATCCATCAGGTTGGACTCG
CTLA4_+6524_RV	AACACTGCCAGCTTTTGGTT
ICOS_-2490_FW	CCTCAGTCAGAAGGGTCGTC
ICOS_-2324_RV	CAGAAATTCCTGGTCATGTTTT
ICOS_+605_FW	AGTCTGCCATAGGGTTGGTG
ICOS_+769_RV	TCAGTCATTTTCTCCCCCTTT
IL10_-172_FW	TCTTTAGCGCTTACAATGCAAA
IL10_-10_RV	CTGTTCTTGGTCCCCCTTTT
ITK_RT_FW	GCATCCCGTGCCACTATAAAT
ITK_RT_RV	CTGCCGACTCTCACAGTCTG
IRF9_RT_FW	CCTCAGGCAAAGTACGCTG
IRF9_RT_RV	GGGGTGTCCTATGTCCCCA
MEF2D_PAN_RT_FW	CCCGTTGGGAATGGCTATGT
MEF2D_PAN_RT_RV	TTAACCCTTTGCCTCCCTGG
MEF2DA1_FW_RT	AGCTGGATGGGCTCTTCAG
MEF2DA1_RV_RT	CAGCATGGCTCCTGCACTA
MEF2DA2_FW_RT	CCAGACGGAAGAGAAGTAT
MEF2DA2_RV_RT	TGACATAGCCATTCCCAACG

Figure 1. Foxp3 controls Mef2d transcription and influences Mef2d protein-protein interactions. A. qPCR results in Treg and Teff from WT mice (n=4, t test). **B**. Immunoblots of indicated proteins in Treg and Teff cells from WT mice. **C.** Phosphorylation sites retained or lost in Mef2d α1 and α2 isoforms. **D.** qPCR in freshly isolated WT Teffs and Tregs or cells cultured under activating conditions for 24 h (1:1 ratio CD3/CD28 mAb-coated beads); n=6, Tukey's multiple comparison test. **E.** Immunoblots of indicated proteins in same cells as Fig. 1D. **F.** Densitometric analysis relative to Fig. 1E; n=2, t test relative to TE. **G.** qPCR results of *Mef2d* (pan, α1, α2) expression in freshly isolated WT Teffs and Tregs or cultured under activating conditions for 60 h in presence of 5 μM Scr or Foxp3 antisense; n=3, Tukey's multiple comparison test. **H.** Immunoblots of indicated proteins in same cells as in Fig. 1G. **I.** Densitometric analysis relative to Fig. 1H. n=2, t test relative to Scr. **J.** HEK-293T cells were transfected with 1μg each of tagged constructs encoding Foxp3, Mef2d and p300; lysates were pulled down with anti-Myc or IgG Ab (1 μg). Film was probed with biotinylated anti-Foxp3 mAb, anti-HA for p300 and anti-myc for Mef2d. **K.** HEK-293T cells were transfected with 1 μg each of FLAG-Foxp3 and depicted deletion mutants of Mef2d-GFP. Lysates were pulled down with anti-GFP Ab (1 μg). **L.** Lysates from freshly isolated or 24 h CD3/CD28 stimulated Teffs and Tregs were pulled down with anti-Mef2d or IgG Ab (1 μg). **M.** Lysates from freshly isolated Tregs were pulled down with anti-Mef2d α1 or anti-Mef2d α2 or IgG Ab (1 μg). **N.** HEK-293T cells were transfected with 1 μg each of tagged constructs encoding Foxp3, Mef2d α1, Mef2d α2 and Hdac9. Lysates were pulled down with anti-Mef2d α1, Mef2d α2 or IgG Ab (1 μg). **O.** Lysates from freshly isolated Tregs were pulled down with anti-Foxp3 or IgG Abs (1 μg); 1/50 input included in all IP.

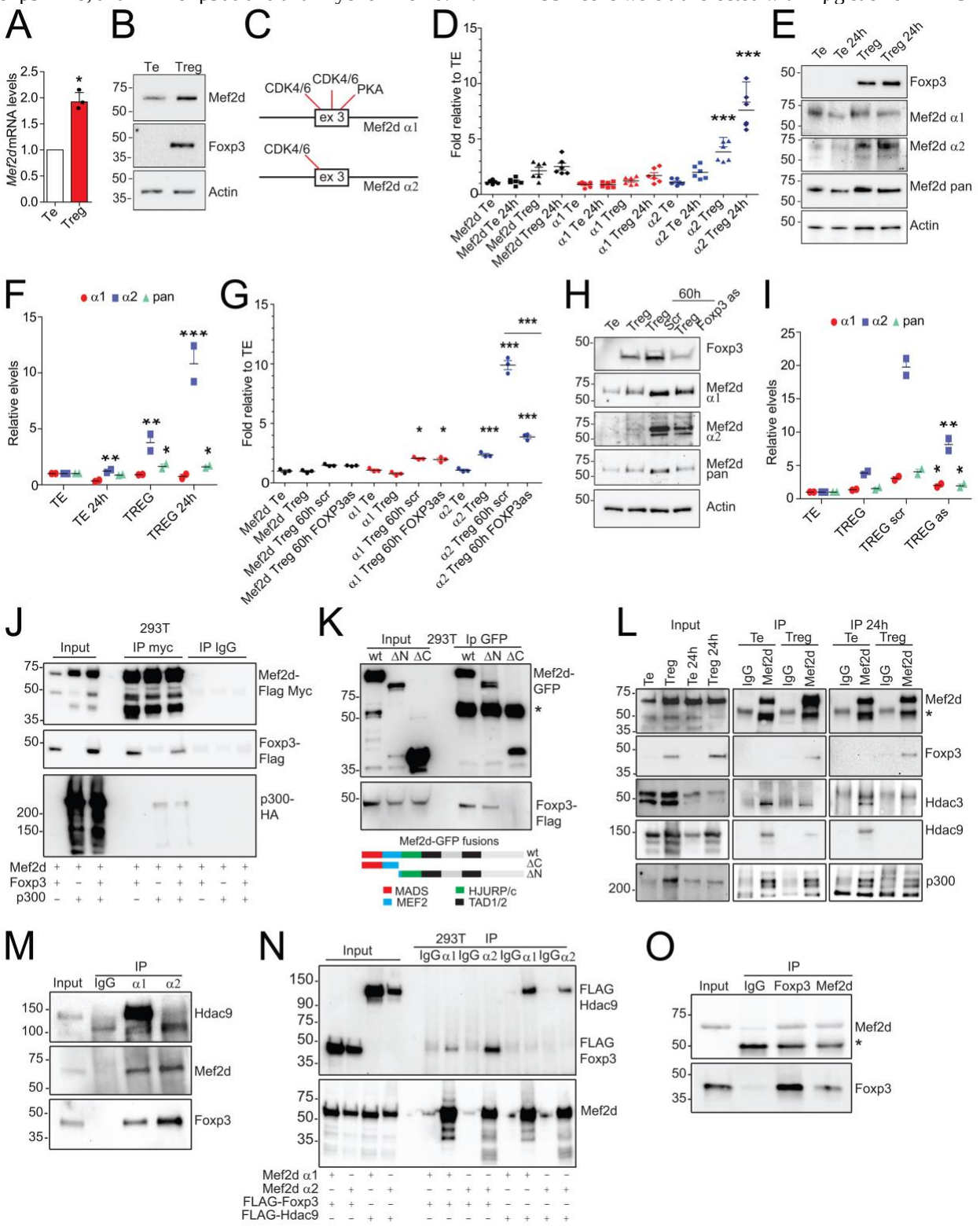

Figure 2. Generation and characterization of mice conditionally deleted for Mef2d in Foxp3+ Treg cells. A. Immunoblots of Mef2d α1/α2 and Hdac9 in freshly isolated Teffs and Tregs obtained from WT and Mef2d-/- mice, as indicated; β-actin loading control. **B-C.** Analysis of CD4+Foxp3+ in lymphoid tissues from Mef2d-/- or WT mice (n=3); the experiment was repeated two times with three mice/group with similar results (*p<0.05, **p<0.01, t-test). **D-G.** Analysis of CD4+CD69+ and CD4+/CD44$_{hi}$CD62L$_{lo}$ + in CD4+/YFP- populations in lymphoid tissues from Mef2d-/- or WT mice (n=3); the experiment was repeated two times with three mice/group with similar results (*p<0.05, **p<0.01, t-test). **H-I.** *In vitro* Treg suppression assay using pooled (4 mice/group) Tregs from lymph nodes and spleens of Mef2d-/- or WT mice and WT T cells; the percentage of WT proliferating cells is shown in each panel. An experiment was run in triplicate and repeated at least 3 times, and the results of a representative experiment are shown. **J.** AUC ratios (KO/WT, one-sample T test with theoretical mean = 1) of three Treg suppression assays performed on CFSE-labeled WT splenocytes as responder cells. The suppressive effects on CD4 and CD8 responders were evaluated after CD4 and CD8 immunostaining.

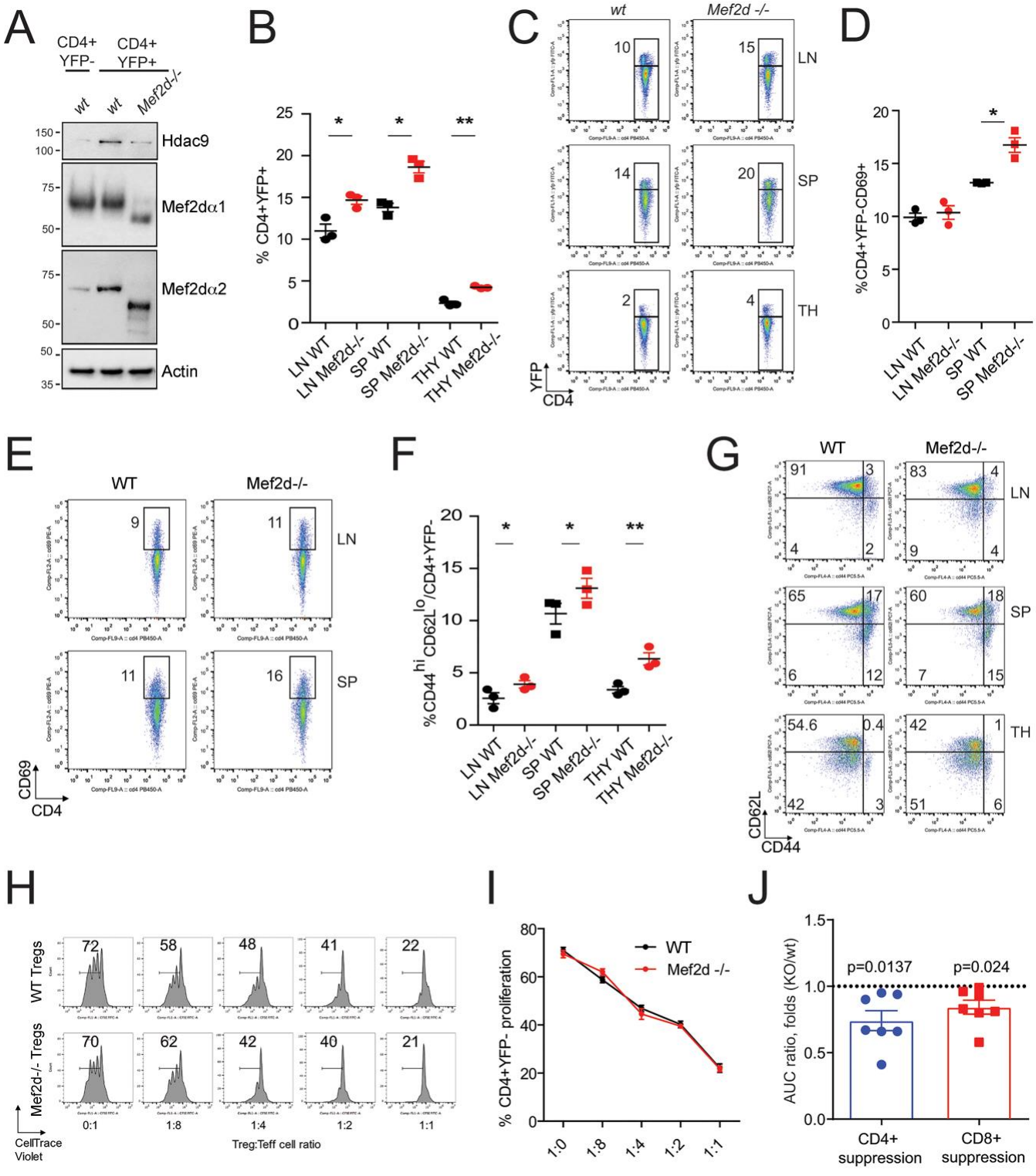

Figure 3. Mef2d deletion affects general and Foxp3 specific responses. A. Volcano plot showing statistical significance (P value) vs. fold change for genes differentially expressed as a result of Mef2d deletion in Foxp3+ Treg cells. **B-F.** GSEA plots obtained by using the indicated gene-sets and the RNA-seq data obtained from the comparison between Mef2d-/- or WT mice Tregs as dataset. **G.** qPCR results of the expression of the indicated genes in freshly isolated Mef2d-/- or WT Teffs and Tregs or cultured under activating conditions for 24 h (1:1 ratio of CD3/CD28 mAb-coated beads); n=5 (*p<0.05, **p<0.01, t-test between TE and Treg in unstimulated and stimulated groups.

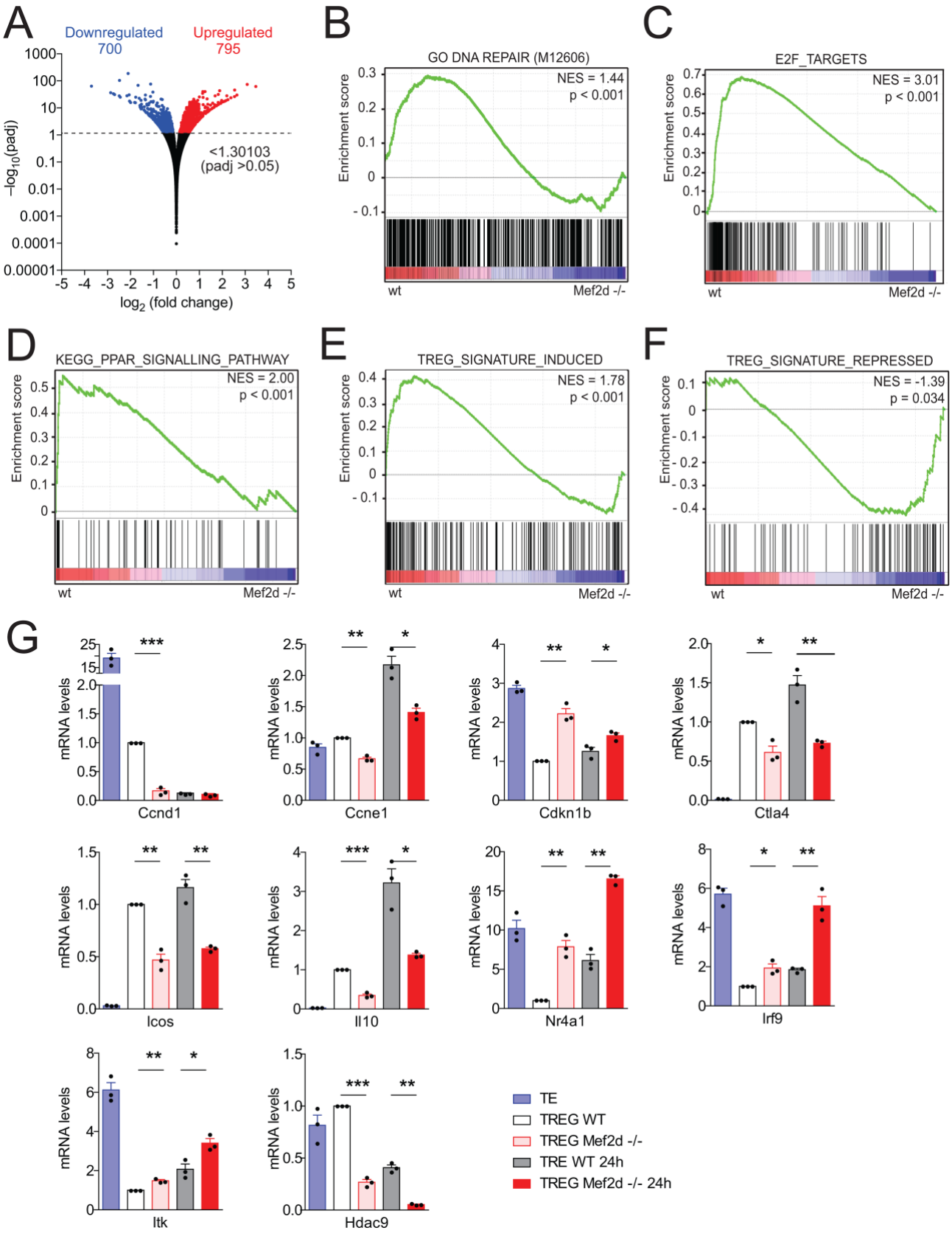

Figure 4. Mef2d deletion perturbs the fitness of Tregs. A. Immunoblots of the expression of the indicated proteins representing key nodes in the identified perturbed pathways in freshly isolated Teffs and Tregs obtained from Mef2d-/- or WT mice, as indicated. β-actin was used as loading control. **-B-D.** Analysis of CD4+Ki67+ in CD4+/Foxp3+ populations in lymphoid tissues from Mef2d-/- or WT mice. n=3, t-test. **C.** Time course analysis of Ki67 positivity in CD4+/Foxp3+ populations purified from Mef2d-/- or WT mice and kept in culture for 3 days with CD3/CD28 mAb-coated beads; n=4, t-test between the two groups for each time point (***p<0.005).

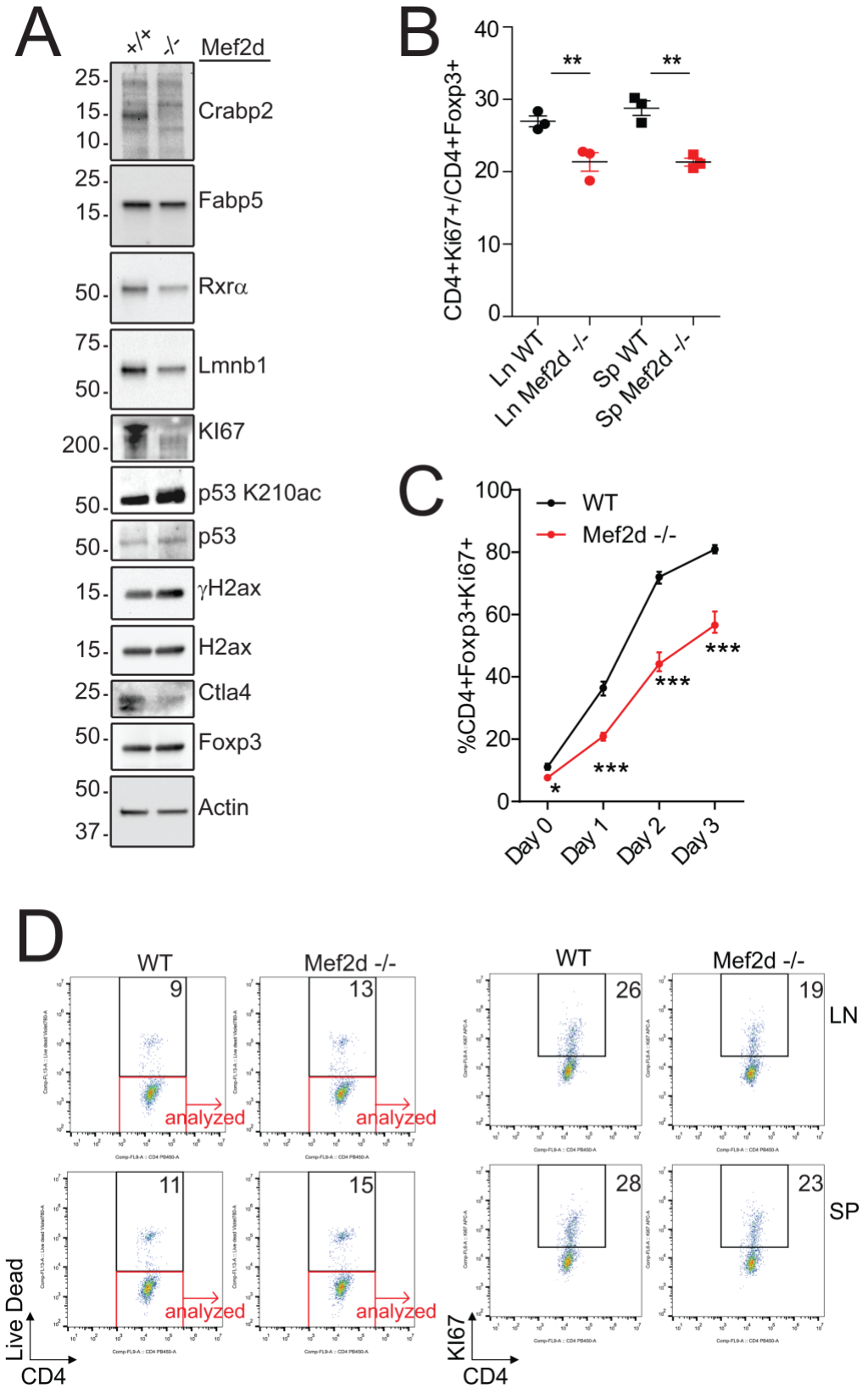

Figure 5. Mef2d is required for the acquisition by Tregs of highly suppressive properties. A-B. GSEA plots obtained by using the indicated gene-sets and the RNA-seq data obtained from the comparison between Mef2d-/- or WT Tregs as dataset. **C.** Heatmap of the expression levels (z-scores) of 10 core genes upregulated in Blimp1+ Tregs in Mef2d-/- or WT Tregs. **D-G**. Analysis of CD4+Foxp3+Ctla4 $_{high}$ (D), CD4+ Foxp3+ Icos$_{high}$ (E), CD4+ Foxp3+ IL-10+ (F-G) populations in lymphoid tissues from Mef2d-/- or WT mice, freshly isolated (D-F) or stimulated with PMA/ionomycin for 4 h (G); the experiment was repeated two times, with three mice/group, with similar results (t test between WT and KO samples, *p<0.05, **p<0.01). **H.** Immunoblots of Blimp1 and Foxp3 in freshly isolated or 24 h CD3/CD28 stimulated Tregs obtained from Mef2d-/- or WT mice, as indicated; β-actin was used as loading control. **I-J.** Representative Treg suppression assay and pooled data (3 mice/group) using Tregs from lymph nodes and spleens of Mef2d-/- or WT mice along with the percentage of proliferating cells in each panel; 48 h before assay, Mef2d-/- or WT Tregs were isolated and stimulated with 1:1 CD3/CD28 coated beads and 10 U/ml IL-2 (t-test between the two groups for each condition, *p<0.05, **p<0.01).

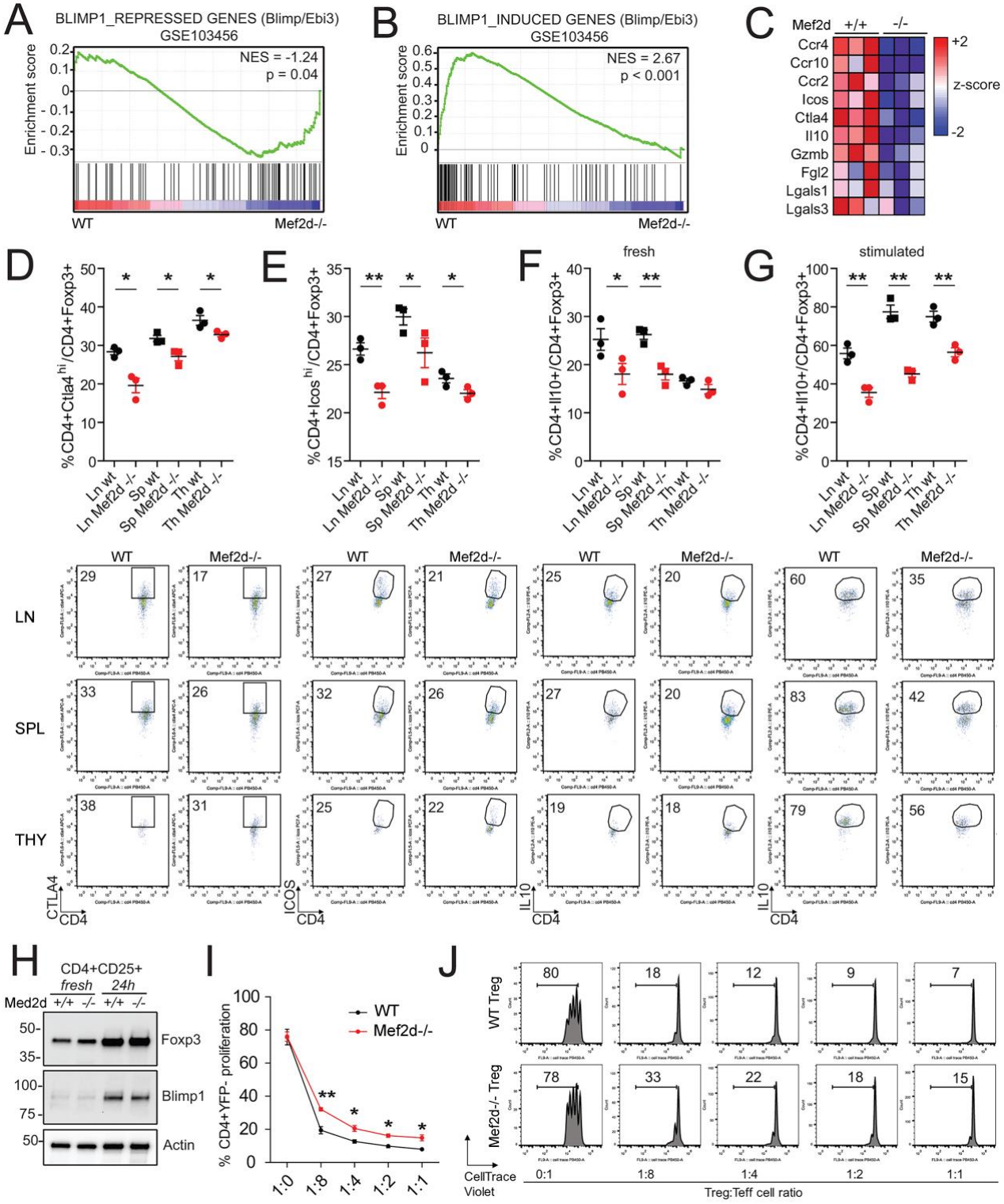

Figure 6. Mef2d deletion dampens Tfr functions partially affecting the Tfh-mediated regulation of B-cell maturation. A-B. Analysis of Tfr (CD4+ CXCR5+ PD1+ Foxp3+) and Tfh (CD4+ CXCR5+ PD1+ Foxp3-) populations in lymphoid tissues from Mef2d-/- or WT mice. n=5. (t test between WT and KO samples, **p<0.01). **C.** Analysis of B cells (CD19+), Memory B cells (CD19+ B220+ $CD62_{low/-}$ FAS- GL7- CD138-) and Plasma cells (CD138+ IgM-) populations in lymphoid tissues from Mef2d-/- or WT mice. n=5, t test between WT and KO samples. **D-I**. Analysis of B cell subpopulations in lymphoid tissues from Mef2d-/- or WT mice. D: B1 cells (B220- CD19+); E: Follicular B cells (CD19+ B220+ CD93-$CD21_{low}CD23_{high}$), Follicular B type I cells (CD19+ B220+ CD93-$CD21_{low}CD23_{high}/IgM_{low}$), Follicular B type II cells CD19+ B220+ CD93- $CD21_{low}CD23_{high}$ IgM_{high}); F: MZ precursor B cells (CD19+ B220+ CD93-$CD21_{high}CD23_{low}$), MZ B cells (CD19+ B220+ CD93- $CD21_{high}CD23_{high}$); H: T1 B cells (CD19+ B220+ CD93+ IgM++ CD23-), T2 B cells (CD19+ B220+ CD93+ IgM++ CD23+), T3 B cells (CD19+ B220+ CD93+ IgM-CD23+); I: GC B cells (CD19+ B220+ GL7+ FAS+), GL7+ activated B cells (CD19+ B220+ GL7+). n=5. (t test between WT and KO samples, *p<0.05, **p<0.01, ***p<0.001). **J.** Autoantibodies detected in the sera of three WT and three Mef2d-/- mice, using indirect immunofluorescence.

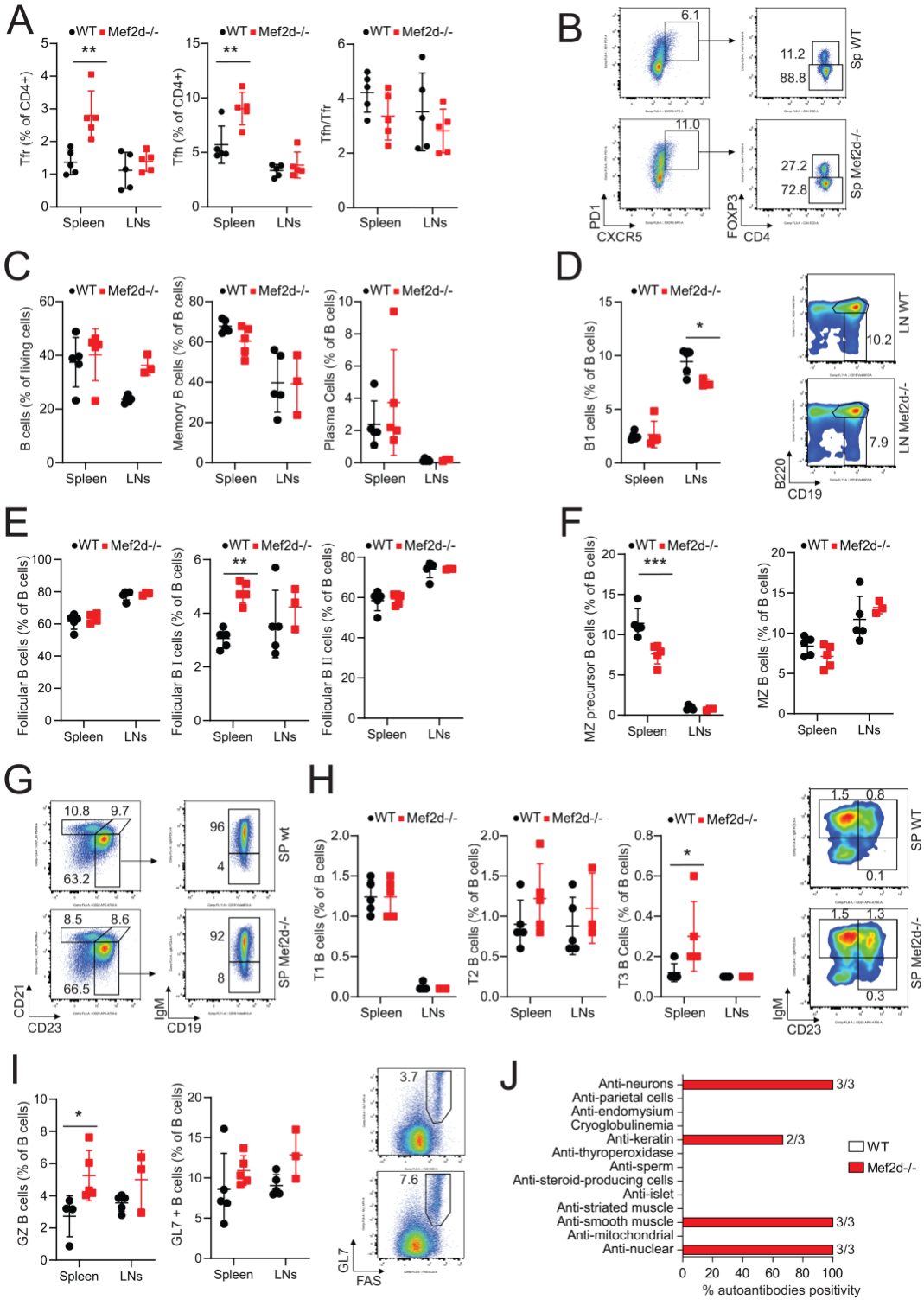

Figure 7. Mef2d-/- Tregs functions are severely impaired *in vivo*. A. 28 days after the adoptive transfer of 0.25x10$_6$ WT Thy1.1+ Teffs and 1.0x10$_6$ WT or Mef2d-/- Thy1.2+ Tregs into *Rag1-/-* mice, splenocytes and lymphocytes were harvested and the total number of Thy1.1+ cells determined by flow cytometry; n=4 (t-test, **p<0.01). **B/C/F.** Analysis of CD4+ Thy1.1+ IFN-γ+ (B) or IL-2+ (C) or Ki67+ (F) populations in lymphoid tissues from the same mice as described in Fig. 7A stimulated with PMA/ionomycin for 4 h; n=4 (t-test, *p<0.05). **D/E.** Analysis of CD4+YFP+ (D) and CD+YFP+CD44$_{high}$/CD62L$_{low}$ Treg populations (E) in lymphoid tissues from the same mice as described in Fig. 7A (t-test, *p<0.05). **G/H.** 28 days after the adoptive transfer of 0.25x106 WT Thy1.1+ Teffs and 1.0x106 WT or Mef2d-/- Thy1.2+ Tregs into Rag1-/- mice, lymphocytes (G) and splenocytes (H) were harvested and the total number of Thy1.1+ cells determined by flow cytometry; n=4. (Tukey's multiple comparison test, *p<0.05, **p<0.01). **I.** In contrast to WT recipients, mice with conditional deletion of Mef2d in their Foxp3+ Treg cells acutely rejected cardiac allografts (BALB/c->C57BL/6) despite costimulation blockade with CD154 mAb/DST; n=5/group (Tukey's multiple comparison test , p<0.01). **J/K.** qPCR results of the expression of the indicated genes in samples collected 2 weeks post-cardiac allografting in WT and Mef2d-/- mice. n=12 and 9, respectively for WT and Mef2d-/- (t-test, *p<0.05, **p<0.01).

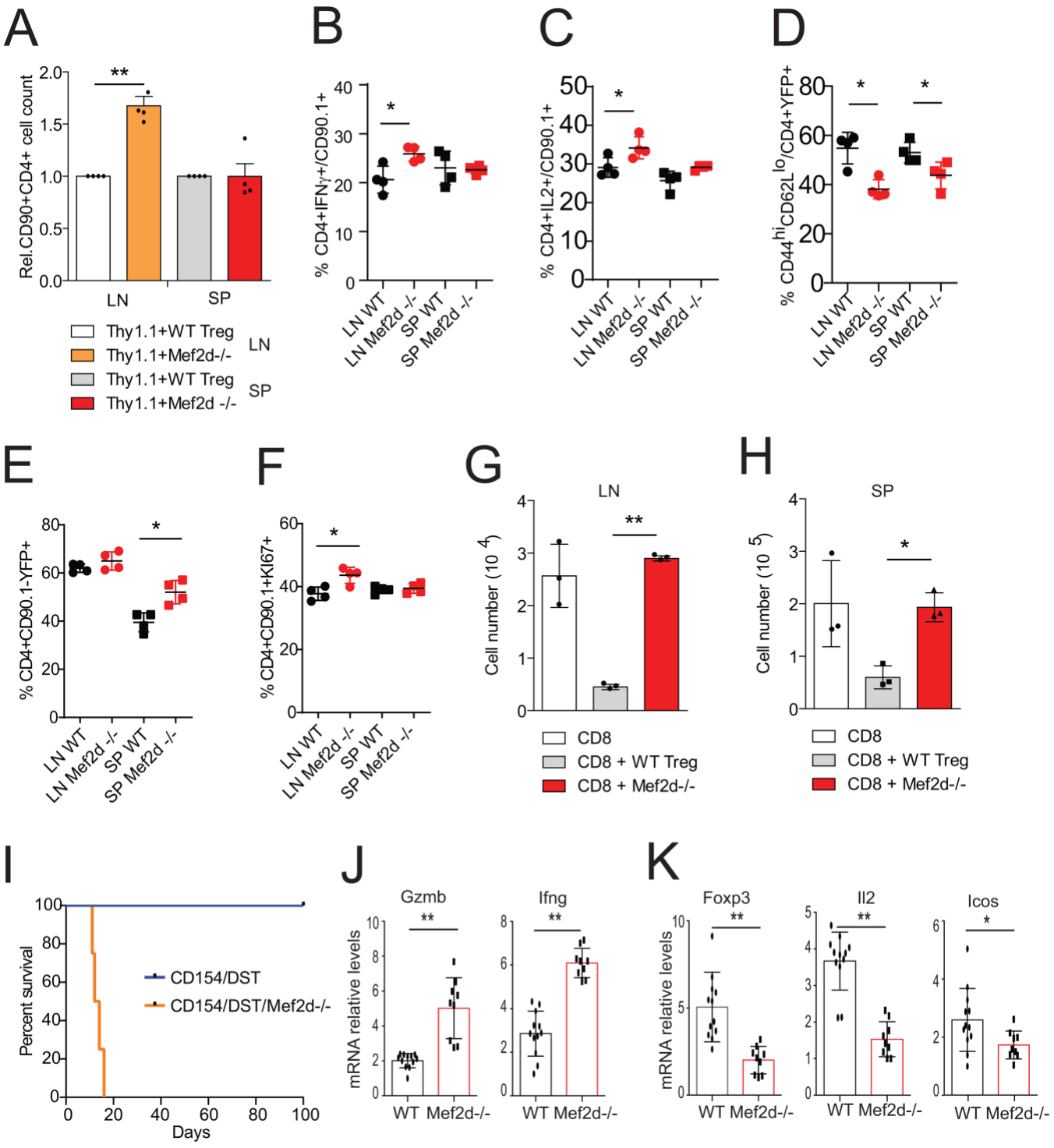

Figure 8. Mef2d deletion promotes anti-cancer immunity in mice bearing subcutaneous lung cancers. A. Graphs representing the tumor growth (volume) in 10 WT and 10 Mef2d-/- mice during a period of 20 days after the subcutaneous injection of $1.2x10_6$ TC1 cells. The experiment was repeated twice with similar results (t-test between the two groups for each time point). **B-C.** Analysis of the activation status of CD4+Foxp3- populations in the same samples as Fig. 8A. **D-I.** Analysis of CD4+Foxp3-IFN-γ+ (D/E), CD8+IFN-γ+ (F/G) and CD8+GZMB+ (H/I) populations in single-cell suspensions obtained from the draining lymph node and spleen harvested from three representative mice injected as in Fig. 8A and stimulated for 4 h with PMA/ionomycin. n=3-5, t-test **J.** CD8 HPV-TC1 specific tetramer staining (E7) positivity in in spleens (SP) and tumor draining LN (TDLN) of WT and Mef2d-/- mice analyzed 10 and 20 days after TC1 cells injection. (t-test, ***p<0.001). **K-L.** Analysis of tumor infiltrating CD4+ Foxp3+ (K) or CD4+ IFN-γ+ (K/L) or CD8+ IFN-γ+ (K/L) populations in tumors harvested from 4 mice per group 8 days after the injection of TC1 cells as in Fig. 8A. n=4, t-test. **M.** Graphs representing the tumor growth (volume) in 10 WT and 10 Mef2d-/- mice during a period of 21 days after the subcutaneous injection of $2.0x10_6$ AE.17 cells, t-test. **N.** Analysis of CD8+ IFN-γ+ populations in single-cell suspensions obtained from the draining lymph nodes and spleen harvested from mice injected with AE.17 cells (n=10, t-test). Where indicated, *p<0.05, **p<0.01, ***p<0.005.

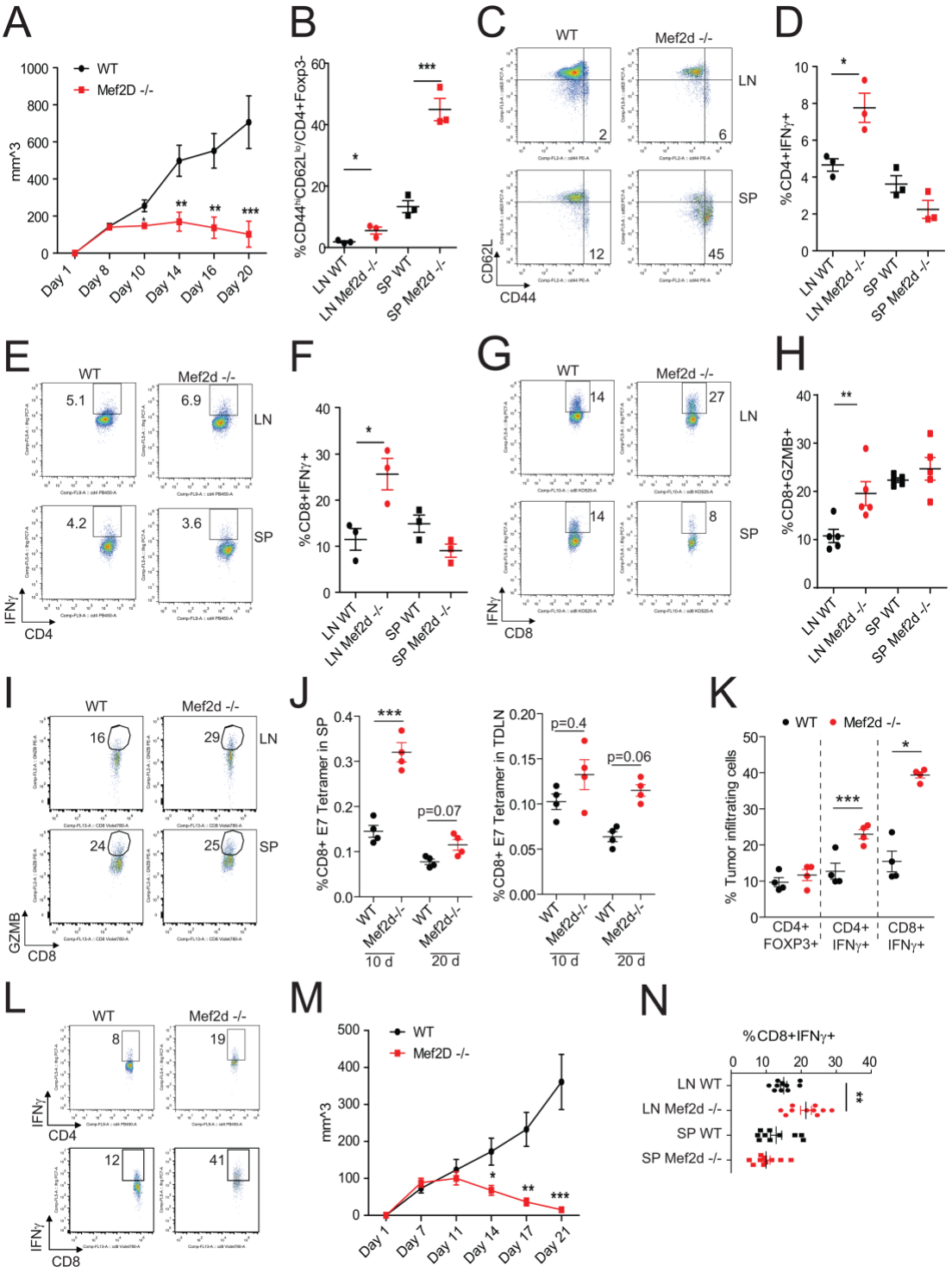

Figure 9. Mef2d deletion promotes anti-cancer immunity in mice bearing HCC. This Figure involves analysis at day 9 after tumor cell injections, and additional data at 21 days post-injection are shown in Supplemental Fig. 11. **A.** H&E-stained sections of WT and Mef2d-/- livers 9 days after the injection of $0.3x10_6$ HCC cells into the mesenteric vein; scale bar = 100 µ. Livers from WT show dense tumors, whereas livers from Mef2d-/- mice are tumor-free. **B.** Dot plot representing the AFP serum levels of 3 healthy C57/BL6 mice and 10 WT and 10 Mef2d-/- mice at day 9 post-HCC injection, Tukey's multiple comparison test. **C-F.** Analysis of the activation status of CD4+Foxp3- and CD8 populations in terms of $CD44_{high}/CD62L_{low}$ (C), CD69 (D) and Ki67 positivity (F) and production of IFN-γ (E) in freshly isolated (C/D/f) or PMA/ionomycin (E) cells obtained from lymphoid tissues of HCC injected mice. n=5, t-test. **G-I.** Analysis of the expression of Ki67 (G), Ctla4 (H) and IL-10 (I) in CD4+Foxp3+ populations in freshly isolated (G) or PMA/ionomycin stimulated (H-I) single-cell suspensions obtained from the same samples of Fig. 9C. n=5, t-test. **J.** qPCR results of the expression of the indicated genes in YFP+ Tregs obtained from the draining lymph nodes of WT and Mef2d-/- HCC injected mice; n=3-5, t-test. **K.** Immunoblots of Ki67, Crabp2, Fabp5 and Ctla4 in the same cells described in Fig. 8Q; β-actin loading control (*p<0.05, **p<0.01, ***p<0.005).

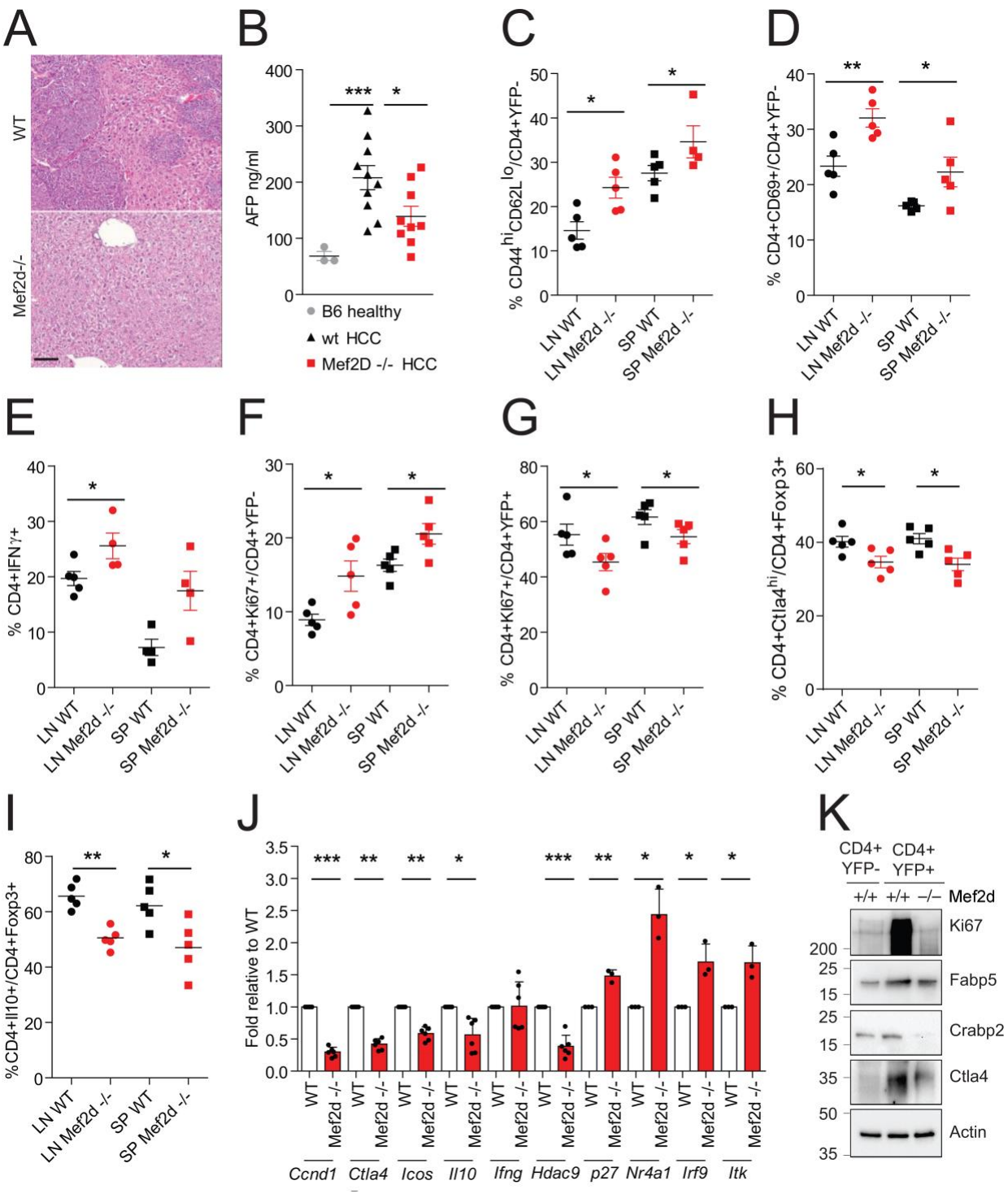

Figure 10. Mef2d works synergistically, additively and independently from Foxp3 in regulating the expression of the bound loci. **A-K.** Histogram representing the qPCR results obtained in freshly isolated WT and Mef2d-/- Tregs after the ChIP with the indicated antibodies. For each investigated genomic locus, a red square indicates the position of the amplified region in respect to the leading TSS and the exons of the associated canonical mRNA isoform (n=2-5). We marked with black asterisks the significance of the indicated comparisons or with respect to the IgG, and with red asterisks the significance of the comparison of the same IP between WT and Mef2d-/- Tregs (*p<0.05, **p<0.01, ***p<0.005, t-test and Tukey's multiple comparison test). **L.** Heatmap representing for each genomic locus the strength of MEF2D and H3K27ac signals in WT and Mef2d-/- Tregs in respect to WT Teffs.

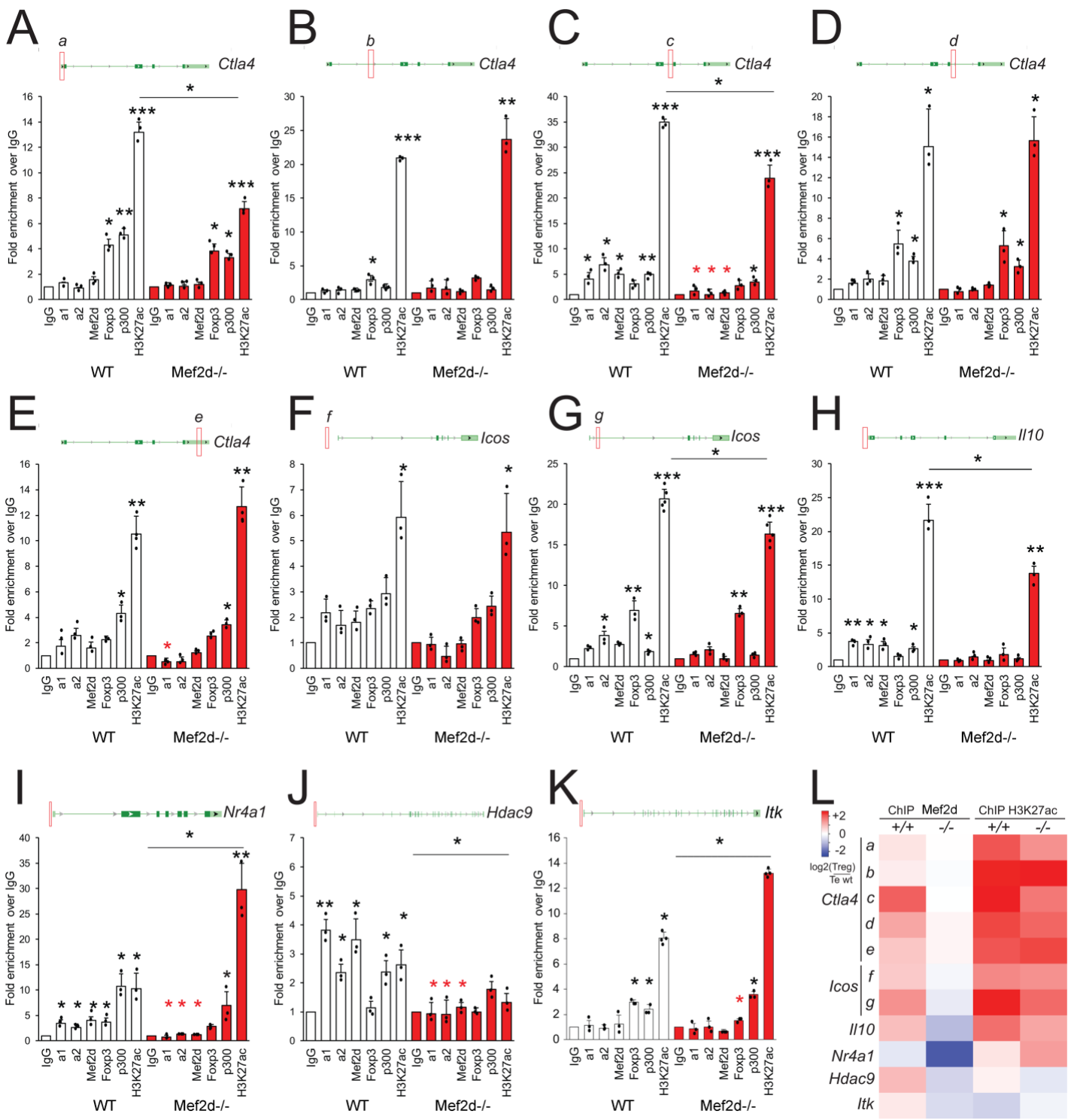

Supplemental Figure Legends

Supplemental Figure 1. Genomic regulation of the Mef2d locus in Tregs. A-B. Absolute levels of Mef2 paralogs in human (A) and murine Tregs (B). Data were derived from our RNA-seq experiment (A) or from Niedzielska et al (82). **C-D.** Foxp3 ChIP-seq signals in human (C) and murine (D) Mef2d locus. **E.** Comparison of H3K27ac and H3K26me3 levels in Mef2d locus between human Tconv and Treg cells; data were retrieved from http://cistrome.org/db.

Supplemental Figure 2. Mef2d-/- mice displayed mild inflammatory infiltrates in lung and liver. Histology of tissues from Mef2d-/- mice at 8 weeks of age showed mild mononuclear cell infiltrates (arrows) in (A) bronchovascular areas of the lung and (B) portal areas in the liver, whereas sections of (C) pancreas, (D) skin, (E) thymus and (F) colon were normal; H&E stained paraffin sections, bar = 100 µM.

Supplemental Figure 3. Relevant pathway alterations characterize Mef2d -/- Tregs. A-E. Heat-map of the expression levels in WT and Mef2d-/- Tregs of core genes belonging to the indicated MsigDB gene sets. Data were expressed as z-score (from blue: -2 to red: +2).

Supplemental Figure 4. Analysis of Mef2d -/- Tregs proliferation and suppressive properties *ex vivo* and *in vivo*. A. Analysis of Ki67 positivity in CD4+/Foxp3+ populations purified from Mef2d-/- or WT mice and kept in culture for 3 days with CD3/CD28 mAb-coated beads. **B-C.** The proliferation score of WT and Mef2d-/-Tregs was calculated after three days of CD3/CD28 stimulation and staining with Cell trace Violet (n=3, t-test). **D-E.** Analysis of Ki67 positivity in CD4+/Foxp3+ populations purified form Rag1-/- mice injected with WT or Mef2d-/- Tregs and Teffs, as described in fig. 7A. **F.** Superimposition of WT and Mef2d-/- flow dot plots and MOF, as described and represented in fig. 5D/G. Light blue and red spots and lines indicated respectively the signals collected in WT and Mef2d-/- samples.

Supplemental Figure 5. Mef2d acts down-stream to Blimp1 to sustain eTreg features. A/C. Relative expression levels of the indicated genes in Blimp1 KO vs WT (A) and Blimp1 + vs – (C) Tregs retrieved from GSE84827 and GSE103456. **B.** Lysates generated from freshly isolated Tregs were pulled down with anti-Blimp1 or IgG antibodies (1 µg). The film was probed with the indicated antibodies; 1/100 inputs are included. **D.** Apoptotic rate was scored in Tregs cells cultured for three days under stimulating conditions by means of annexin V/7-AAD staining (n=3, t-test *p<0.05). **E.** Caspase 3 cleavage was detected in lysates generate from stimulated Tregs as in Supplemental Fig. 4C. β-actin was used as loading control. **F-I.** Treg suppression assay using pooled (3 mice/group) IL-2 expanded Tregs from lymph nodes and spleens of WT and Mef2d-/- mice. For IFN-γ production, cells were stimulated at day 3 for 4 h with PMA/ionomycin (n=3). **J.** Indirect immunofluorescence of cryosections of WT C57/BL6 murine tissues, incubated with serial dilutions (1:1-1:80) of WT and Mef2d-/- sera and secondary anti-mouse FITC antibodies. Arrows point to positive signals evidenced by using Mef2d-/- sera, but not WT sera. The signal intensity and exposure were compared to previously characterized positive and negative controls.

Supplemental Figure 6. Impairment of Mef2d-/- Tregs *in vivo*. A-E. Flow data panel relative to the adoptive transfer described in Fig. 7A. A/B/E. Analysis of CD4+ Thy1.1+ IFN-γ+ (A) or IL-2+ (B) or KI67+ (E) populations in lymphoid tissues from the same mice as described in Fig. 7A stimulated (A/B) or not (E) with PMA/ionomycin for 4 h; n=4 (t-test, *p<0.05). C/D**.** Analysis of CD4+YFP+ (C) and CD4+YFP+CD44$_{high}$/CD62L$_{low}$ (D) Treg populations in lymphoid tissues from the same mice as described in Fig. 7A (t-test, *p<0.05). **F.** RNA expression levels of the indicated chemokine receptors in Mef2d-/- Tregs, expressed as log2 (fold KO/wt), after normalization to levels in WT Tregs (dotted line).

Supplemental Figure 7. Histology of allografts at day 14 post-Tx. Cardiac allografts were performed (BALB/c->C57BL/6) with CD154 mAb/DST at engraftment. Left panels from WT recipients show mild mononuclear cell infiltrates, intact myocardium and vessels (arrows). By contrast, grafts in Mef2d-/- recipients

(right panels) show severe injury with myocardial necrosis, interstitial hemorrhages, mixed leukocytic infiltrates, and necrotizing vascular injury (arrows) and fibro-intimal proliferation.

Supplemental Figure 8. Vascular deposition of C4d at day 14 post-Tx (BALB/c->C57BL/6) and CD154/DST. **A**. Lack of C4d deposition on endothelium of vessels of WT recipients treated with CD154/DST. **B**. Lack of staining with control primary antibody (Mef2d-/- recipient). **C**. C4d deposition on endothelial cells in a vessel not subject to fibro-intimal thickening (Mef2d-/- recipient). **D**. Extensive C4d deposition in a vessel with fibro-intimal thickening (Mef2d-/- recipient). Immunoperoxidase with DAB substrate and hematoxylin counterstain. Bar = 100 μM.

Supplemental Figure 9. Mef2d role in anti-cancer immunity. A-F. Analysis of the expression of Ctla4 (A/B), IL-10 (C/D) and Ki67 (E/F) in CD4+Foxp3+ populations in freshly isolated (A/B, E/F) or PMA/ionomycin stimulated (C/D) single-cell suspensions obtained from the same samples as Fig. 8A. n=3, t-test. **G.** qPCR results of the expression of the indicated genes in freshly isolated WT and Mef2d-/- CD4+YFP+ cells harvested from the draining lymph nodes of TC1 tumor bearing mice (n=3, t-test *$p<0.05$, **$p<0.01$). **H.** Analysis of tumor infiltrating CD8+CD69+ populations in tumors harvested from 4 mice per group 8 days after the injection of TC1 cells as in Fig.8A. n=4, t-test. **I-J-K.** Analysis of CD8+ IFN-γ+ (I) and CD4+ Foxp3- IFN-γ+ (J/K) populations in single-cell suspensions obtained from the draining lymph node and spleen harvested from three representative mice injected as in Fig. 8M and stimulated for 4 h with PMA/ionomycin (n=10, t-test **$p<0.01$).

Supplemental Figure 10. The depletion of Mef2d in Tregs modulates TE and Tregs functions in anti-cancer immunity. A-D. Analysis of the activation status of CD4+Foxp3- and CD8 populations in terms of CD44high/CD62Llow (A), CD69 (B), Ki67 positivity (D) and production of IFN-γ (C) in freshly isolated (A/B/D) or PMA/ionomycin (C) cells obtained from lymphoid tissues of HCC injected mice. Data refers to Fig. 9C-F. **E-G.** Analysis of the expression of Ki67 (E), Ctla4 (F) and IL-10 (G) in CD4+Foxp3+ populations in freshly isolated (E/F) or PMA/ionomycin stimulated (G) single-cell suspensions obtained from the same samples of Fig. 9G-I. **H-**

J. Analysis of CD8+CD69+ (H), CD8+ IFN-γ+ (I) and CD4+ Foxp3- IL-2+ (J) populations in single-cell suspensions obtained from the draining lymph node and spleen harvested from five representative mice injected as in Fig. 9B and stimulated for 4 h with PMA/ionomycin.

Supplemental Figure 11. HCC data at day 21 post-injection. Upper panels show macroscopic tumors in 3 Cre control mice in contrast to the absence of tumors in Mef2d-/- mice, plus corresponding AFP data (***$p<0.001$). Lower panels show histologic confirmation of HCC tumors in the same mice (H&E-stained paraffin sections, bar = 50 μ), with individual AFP levels shown; arrows indicate tumor masses, including with complete overgrowth of the liver by tumor cells in Cre control #3 (single arrow).

Supplemental Figure 12. Highlight on the genomic locus of Ctla4/Icos. A. Hi-C data, Foxp3 and H3K27ac levels in Ctla4/Icos locus with the indications of the investigated regions in ChIP experiments (Fig. 9). Data were retrieved from http://cistrome.org/db and http://promoter.bx.psu.edu/hi-c/view.php. **B-C.** Histograms representing the qPCR results obtained in freshly isolated WT Teffs after the ChIP with H3K27ac (B) and MEF2D (C) antibodies. n=3, t-test; asterisks show the significance of the indicated comparisons with respect to control IgG (*$p<0.05$, **$p<0.01$, ***$p<0.005$).